Vol. 01 No. 02 2023

RiESTech

JOURNAL RECENT IN ENGINEERING SCIENCE AND TECHNOLOGY

MBI

E- ISSN : 2985-8321
P -ISSN : 2985-704X

Recent in Engineering Science and Technology (RiESTech)
PT MENCERDASKAN BANGSA INDONESIA (MBI)
Available online at: http://www.mbi-journals.com/index.php/riestech

E- ISSN : 2985-8321
P -ISSN : 2985-704X

Recent in Engineering Science and Technology (RiESTech)

Volume 1 No 2 April 2023

FOCUS AND SCOPE

RIESTECH

Recent in Engineering Science and Technology **(RiESTech):** I*SSN: 2985-704X (print), ISSN: 2985-8321 (online)* a peer-reviewed quarterly engineering journal, publishes theoretical and experimental high-quality papers to promote engineering and technology's theory and practice. In addition to peer-reviewed original research papers, the Editorial Board welcomes original research reports, state-of-the-art reviews, and communications in the broadly defined field of recent engineering science and technology. **RiESTech** covers topics contributing to a better understanding of engineering, material science, computer science, environmental science, and their applications. **RiESTech** is concerned with scientific research on mechanical and civil engineering, Electrical/Electronics and Computer Engineering, and Metallurgical and Materials Engineering with specific analytical techniques and/or computational methods.

The frequency of RiESTech publications is four times a year namely in January, April, July, and October. The scope of RiESTech includes a wide spectrum of subjects namely:

Mechanical and Civil Engineering (Automotive Technologies; Construction Materials; Design and Manufacturing; Dynamics and Control; Energy Generation, Utilization, Conversion, and Storage; Fluid Mechanics and Hydraulics; Heat and Mass Transfer; Micro-Nano Sciences; Renewable and Sustainable Energy Technologies; Robotics and Mechatronics; Solid Mechanics and Structure; Thermal Sciences)

Electrical/Electronics and Computer Engineering (Instrumentation; Coding, Cryptography, and Information Protection; Communications, Networks, Mobile Computing, and Distributed Systems; Compilers and Operating Systems; Parallel Processing, and Dependability; Computer Vision and Robotics; Control Theory; Electromagnetic Waves, Microwave Techniques and Antennas; Embedded Systems; Integrated Circuits, VLSI Design, Testing, and CAD; Microelectromechanical Systems; Microelectronics, and Electronic Devices and Circuits; Power, Energy and Energy Conversion Systems; Signal, Image, and Speech Processing; Machine Learning and Data Science)

E- ISSN : 2985-8321
P -ISSN : 2985-704X

Metallurgical and Materials Engineering (Advanced Materials Science; Ceramic and Inorganic Materials; Electronic-Magnetic Materials; Energy and Environment; Materials Characterization; Metallurgy Extractive; Polymers and Nanocomposites)

Environmental Science and Engineering (Waste Management, Climate Change, Zero Waste, Environmental Disaster Management, Circular Economy, Sustainable Development, Environmental Security, Environmental Management, Environmental Ecology, Conservation of Natural Resources And Environment, Environmental Impact Analysis, Planning and Environmental Administration, Environmental Health, Environmental Pollution, Environmental Accounting, and Environmental Information Systems)

Recent in Engineering Science and Technology (RiESTech)
PT MENCERDASKAN BANGSA INDONESIA (MBI)
Available online at: http://www.mbi-journals.com/index.php/riestech

E- ISSN : 2985-8321
P -ISSN : 2985-704X

Recent in Engineering Science and Technology (RiESTech)

Volume 1 No 2 April 2023

Recent in Engineering Science and Technology (RiESTech)
PT MENCERDASKAN BANGSA INDONESIA (MBI)
Available online at: http://www.mbi-journals.com/index.php/riestech

E- ISSN : 2985-8321
P -ISSN : 2985-704X

Layout and Typesetting:

Imam Sapto Nugroho, Universitas Indonesia (Alumni), Indonesia
Kamil Raihan Permana, Universitas Indonesia, Indonesia
Raihan Trinanda Agsya, Politeknik Negeri Jakarta, Indonesia

PUBLISHER
PT MENCERDASKAN BANGSA INDONESIA (MBI)
Address : 4th Floor Gedung STC Senayan Room 31-34, Jl. Asia Afrika Pintu IX, Jakarta 10270, Indonesia.

Recent in Engineering Science and Technology (RiESTech)
PT MENCERDASKAN BANGSA INDONESIA (MBI)
Available online at: http://www.mbi-journals.com/index.php/riestech

E- ISSN : 2985-8321
P -ISSN : 2985-704X

Recent in Engineering Science and Technology (RiESTech)

Volume 1 No 2 April 2023

PREFACE

Journal RiESTech (p-ISSN: 2985-704X (print), e-ISSN: 2985-8321 (online); is a peer review journal published by PT Mencerdaskan Bangsa Indonesia. The RiESTech journal is published four times a year in January, April, July, and October. This journal provides direct open access to its content on the principle that making research freely available to the public supports a greater global exchange of knowledge within the engineering field. This journal aims to provide a place for academics, researchers, and practitioners to publish original research articles or review articles. The scope of articles published in this journal relates to various topics in the field of outcomes of research activities.

The RiESTech journal publishes papers strictly following the RiESTech guidelines and templates for manuscript preparation. All submitted manuscripts will go through a double-blind peer review process. The paper is read by members of the editor (according to the area of specialization) and will be screened by the Managing Editor to meet the criteria required for RiESTech publication. Manuscripts will be sent to two reviewers based on their historical experience in reviewing manuscripts or based on their areas of specialization. RiESTech has review forms to keep the same item reviewed by two reviewers. Then the editorial board makes a decision on the comments or suggestions of the reviewers.

Reviewers provide an assessment of originality, clarity of presentation, contribution to the field/science. This journal publishes research articles, review articles/literature reviews, case reports and concept/policy articles, in all fields of Computer Science, Informatics Engineering, Multimedia, Arts. The article to be published is an original work and has never been published. Incoming articles will be reviewed by the reviewer team.

The Editorial Board will try to continue to improve the quality of the journal so that it can become an important reference in the development of engineering sciences. The greatest appreciation and gratitude to Mitra Bestari along with members of the Editorial Board and all parties involved in the publication of this journal. Complete writing instructions are displayed on the portal of this journal.

Regards,

Chief Editor

Recent in Engineering Science and Technology (RiESTech)
PT MENCERDASKAN BANGSA INDONESIA (MBI)
Available online at: http://www.mbi-journals.com/index.php/riestech

E- ISSN : 2985-8321
P -ISSN : 2985-704X

Recent in Engineering Science and Technology (RiESTech)

Volume 1 No 2 April 2023

Contents

Focus and Scope ii
Editor Team iv
Preface vi
Contents vii

Articles

- ***The Modification of the Runner and Ingate Geometry to eliminate Misrun Defects on the Piston using Gravity Die Casting***
  Vika Rizkia, Muhammad Fernanda Alvi Yasin and Nabila Banowati, Veronika Noviaty
  1 - 11
- ***Study on the Structure of GaN films deposited on MoS2/Sapphire via Plasma-Assisted Molecular Beam Epitaxy***
  Iwan Susanto, Chi-Yu Tsai, Nurzal Nurzal, M Zalu Purnomo, Ing-Song Yu
  12 - 18
- ***Electric Vehicle Conversion Study for Sustainable Transport***
  Fuad Zainuri, Muhammad Hidayat Tullah, Sonki Prasetya, Iwan Susanto, Dewin Purnama, Rahmat Subarkah, Tia Ramiati, Widiyatmoko, Rahmat Noval
  19 - 25
- ***Application of AGV in the Production System at the PT. Adhikara Wiyasa Gani***
  Agus Siswoyo, Rodik Wahyu Indrawan, Abdul Azis Abdillah
  26 - 35
- ***Catalytic Graphitization of Biomass as a Potential Method Produce Graphite In The Future : A Review***
  Isnanda Nuriskasari, Anne Zulfia Syahrial, Johny Wahyuadi M Soedarsono
  36 - 45

RiESTech
Recent in Engineering Science and Technology

MBI

Article

The Modification of the Runner and Ingate Geometry to eliminate Misrun Defects on the Piston using Gravity Die Casting

Vika Rizkia [1*], Muhammad Fernanda Alvi Yasin [1*], Nabila Banowati [1], Veronika Noviaty [1]

[1] Mechanical Engineering, Politeknik Negeri Jakarta, Kampus UI, Depok, 16425
* Correspondence: vika.rizkia@mesin.pnj.ac.id ; muhammadfernanda5@gmail.com

Abstract: Piston is an essential component of an engine because it plays a crucial role in the combustion process that drives the motorcycle. Gravity dies casting has become an ideal method for producing pistons owing to its high-quality product, cost-effective with excellent dimensional accuracy, good surface finish, and performance characteristics. However, misrun defect may occur during metal filling and solidification. This study aims to find the suitable dimensions for motorcycle piston products without the presence of misrun using MAGMASoft. The geometry modification introduced in this research are an ingate area of 176, 264, and 352 mm2 as well as the angle of runner of 60, 160, and 180o. Modifying the ingate area to 264 mm2 and the angle of the runner to 160o eliminated the misrun defect in the piston product. This phenomenon results from the laminar flow, higher temperature, and quicker flow velocity of the molten metal as it fills the window (the thinnest part of the piston).

Keywords: Casting; Piston; Runner; Ingate; Misrun Defect

Citation: Rizkia, V., Fernanda Alvi Yasin, M., Banowati, N., & Noviaty, V. (2023). The Modification of the Runner and Ingate Geometry to eliminate Misrun Defects on the Piston using Gravity Die Casting. Recent in Engineering Science and Technology, 1(02), 1–11. https://doi.org/10.59511/riestech.v1i02.13

Academic Editor: Iwan Susanto

Received: 6 February 2023
Accepted: 3 March 2023
Published: 1 April 2023

Publisher's Note: MBI stays neutral with regard to jurisdictional claims in published maps and institutional affiliations.

1. Introduction

The motorcycle piston is a vital component of an engine as it plays a critical role in the combustion process that powers the motorcycle. The piston is responsible for converting the energy from the burning fuel and air mixture into mechanical motion by moving up and down inside the engine's cylinder[1]. Gravity dies casting is an ideal method for producing high-quality, cost-effective pistons with excellent dimensional accuracy, surface finish, and performance characteristics[2]–[4]. However, in addition to the inherent benefits, various defects such as misrun, shrinkage, inappropriate filling, porosity, blow holes, and pin holes may occur during metal filling and solidification[5], [6]. According to reports, ninety percent of these casting flaws result from improper casting design [7]–[10], which influences mold filling and affects the mechanical properties of the cast pieces[11], [12].

Due to the importance of mold filling, numerous studies have been conducted in this field. Mold filling is affected by fluid flow pattern, gating design, and solidification[13], [14]. Masoumi et al. [15] reported that alterations in gating system configuration result in a divergence of melt flow from the mold's parting line, altering the mold filling pattern. According to Rajput et al. [16], gate geometry influences the change of metal head pressure at the mold cavity entrance. The design of the gate influences metal filling, which directly affects casting quality. The correct gating design produces a uniform heat gradient and prevents mold erosion, producing smooth metal flow. Precise gate sizes and designs minimize air entrapment by controlling the entry velocity of molten metal.

In addition, numerous researchers have developed mathematical models to

overcome the casting defects mentioned above [17]–[21]. These mathematical models have been implemented as software. MAGMAsoft is one such program renowned for its virtual casting simulation and optimization capabilities[22]. With such tools, numerical simulations were conducted to identify flaws virtually. These virtual simulations aid in the reduction of casting flaws, which benefits manufacturers in numerous ways. Vijayaram et al. [23] examined computer simulations' use to detect casting defects that develop during the solidification phase of casting components. They demonstrated that such simulations greatly benefited the foundry industry. Gunasegaram et al. [24] determined the essential elements that influence the shrinkage porosity in permanent mold castings utilizing numerical simulation and experimental design to achieve an optimum result. They discovered that a thick mold layer combined with a high mold temperature significantly shifted the shrinkage porosity away from important locations. Dabade et al. [25] employed the design of experiments and the Taguchi technique to identify the main process parameter influencing the casting process. In order to lessen the degree of shrinkage porosity in the cast component, they performed a solidification study with novel gating and feeding systems using computer simulation software. Their results demonstrated a significant decrease in shrinkage porosity and an improvement in casting yield.

Among other similar studies, in this research, the numerical simulation technique was applied to the gravity die casting of a cast component to diminish the misrun defect. The component considered for the investigation was a motorcycle piston. The cast component was realistically simulated using MAGMAsoft, and the simulation results were implemented in real-time casting.

2. Materials and Experiment Methods

The present investigation is performed to find the proper dimensions of the runner and ingate in the motorcycle piston case, which is being processed in the gravity die casting route, and resolve the misrun defects identified using MAGMAsoft. The three-dimensional CAD model and the actual product of the initial piston casting are shown in Figure. 1. In addition, the material specifications and gating system parameters are seen in Table.1.

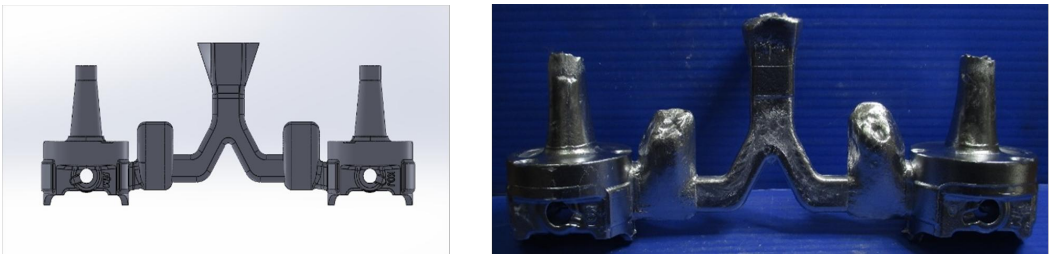

Figure 1. (a) 3D models of the piston and the gating system, (b) as cast piston

Table 1. Material specifications and gating system parameter

Cast Material	A351
Dies Material	H13
Pouring Temperature	760°C
Dies Core Temperature	350°C
Piston weight (1 cavity)	0.6 kg

Piston height	76 mm
Sprue height	67 mm
Ingate area	164 mm^2
Angle of runner	60^o

In this study, the initial design was modified in order to diminish misrun defect within the cast product by changing the ingate area of 176, 264, and 352 mm2 as well as the angle of runner of 60, 160, and 180^0.

3. Results and Discussion

3.1. Flow Tracer

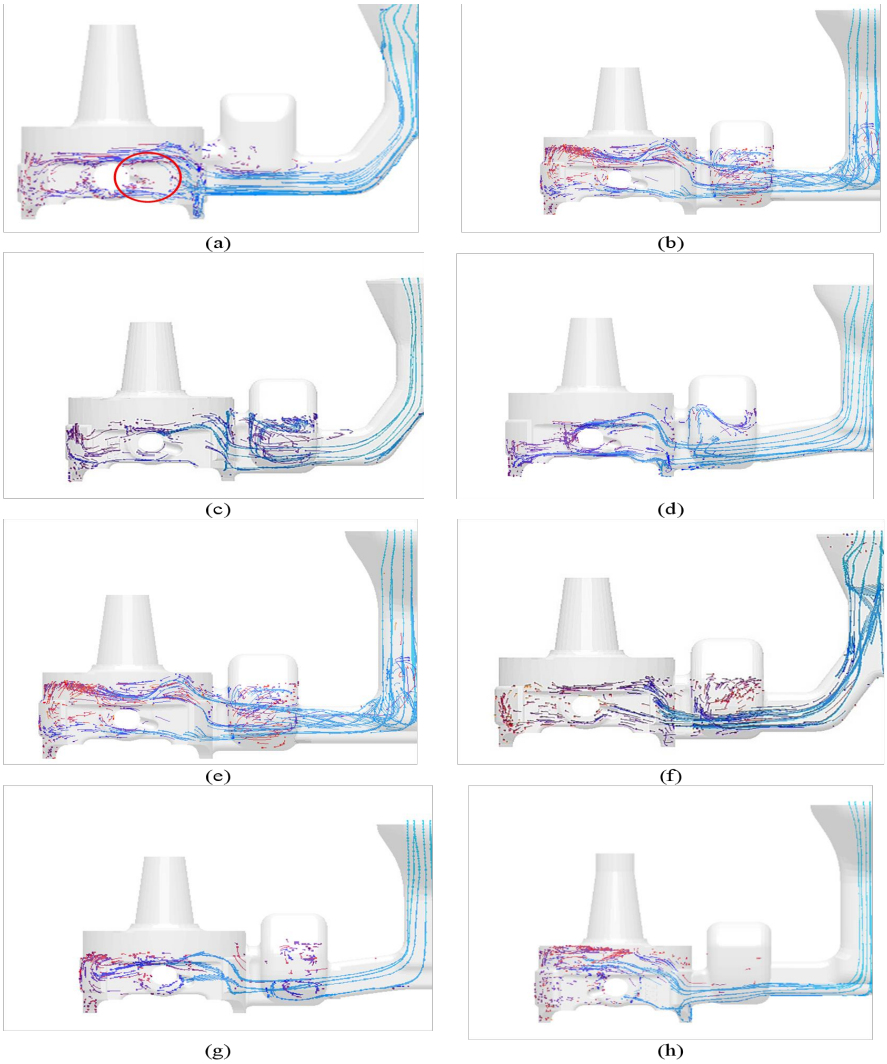

Figure 2. The flow tracer of (a) original design, (b) ingate area of 352 mm2 and angle of the runner of 180^0, (c) ingate area of 352 mm2 and angle of the runner of 60^0, (d) ingate area of 352 mm2 and angle of the runner of 160^0, (e) ingate area of 176 mm2 and angle of the runner of 180^0, (f) ingate area of 176 mm2 and angle of the runner of 60^0, (g) ingate area of 176 mm2 and angle of the runner of 160^0, (h) ingate area of 264 mm2 and angle of the runner of 180^0, (i) ingate area of 264 mm2 and angle of the runner of 60^0, (j) ingate area of 264 mm2 and angle of the runner of 160^0

The flow tracer in MAGMASOFT software illustrates the flow of material that passes through the gating system to be directed toward the product. The flow tracer indicates the presence of turbulence and non-uniform flow of molten metal, which result in a misrun. Figure 2 depicts the flow tracer in both the initial design as well as modified designs. Figure 2(a) demonstrates that the flow direction of the material entering the gate channel towards the product is unevenly distributed. It generates turbulence in the window region, as the red circle indicates. As a result of turbulence in the window section, which is a thinner profile, a misrun can occur because the window section solidifies faster than other parts.

In the 1st – 8th modification designs depicted in Figure 2 (b)-(i), turbulence flow is still present. However, in the 9th modification, which involves changes in the geometry of the ingate area of 264 mm2 and a runner angle of 160o as seen in Figure 2 (j), there is no visible turbulence flow. In addition, in the flow tracer analysis of the 9th modification, the flow of material filling the product is uniform and stable, particularly in the narrow profile area (the window) where defects such as misrun are critical.

3.2. Velocity

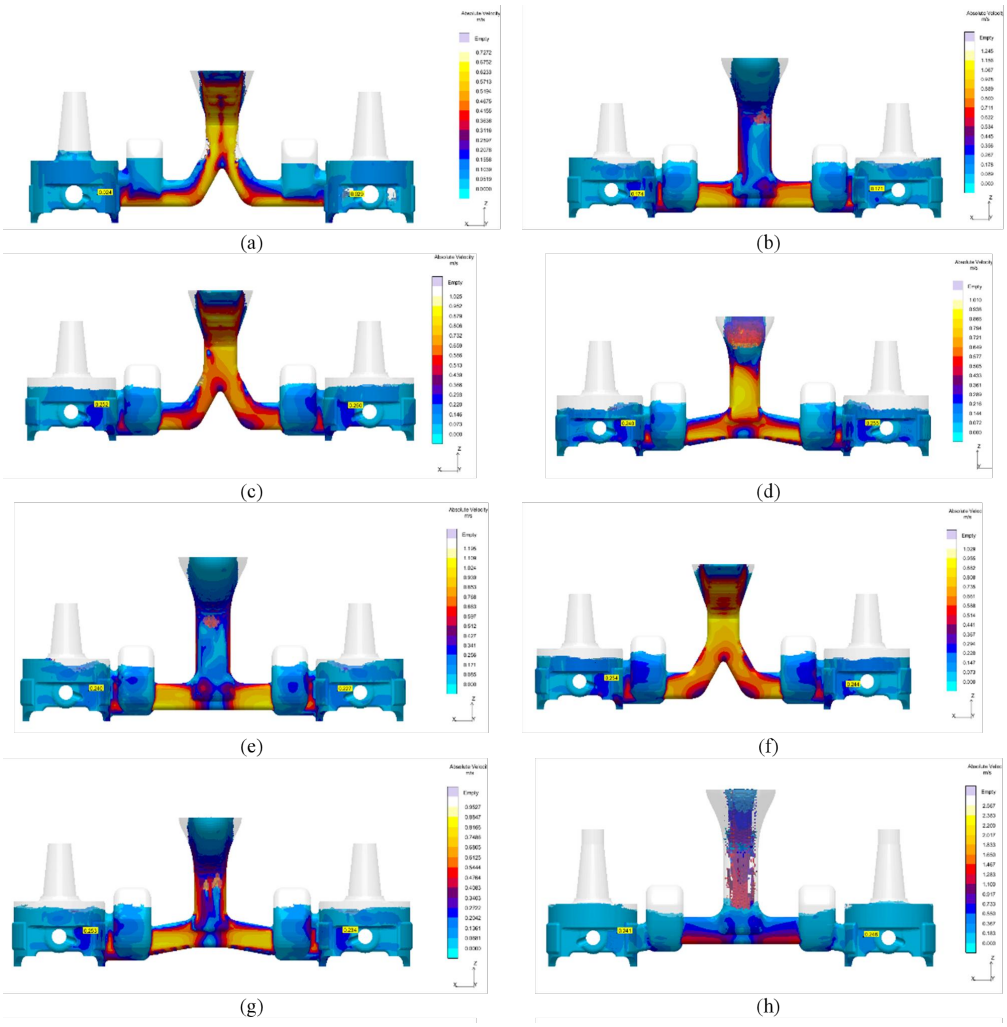

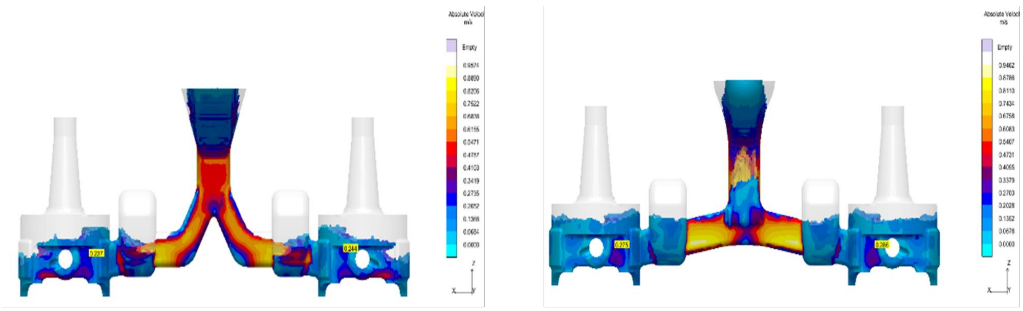

(i) (j)

Figure 3. The flow velocity of (a) original design, (b) ingate area of 352 mm2 and angle of the runner of 180⁰, (c) ingate area of 352 mm2 and angle of the runner of 60⁰, (d) ingate area of 352 mm2 and angle of the runner of 160⁰, (e) ingate area of 176 mm2 and angle of the runner of 180⁰, (f) ingate area of 176 mm2 and angle of the runner of 60⁰, (g) ingate area of 176 mm2 and angle of the runner of 160⁰, (h) ingate area of 264 mm2 and angle of the runner of 180⁰, (i) ingate area of 264 mm2 and angle of the runner of 60⁰, (j) ingate area of 264 mm2 and angle of the runner of 160⁰

The flow velocity in the MAGMASOFT program depicts the material flow rate during mold filling and the spread of the molten flow toward the product. If the flow velocity is low when filling the mold, as in the case of thin profiles or window sections of the product, premature solidification may occur. Figure 3 depicts the flow velocity in both the initial design as well as modified designs. Figure 3(a) demonstrates that molten metal enters the gating system (ingate) unevenly at 1.244 seconds. In addition, a very low flow velocity occurs in the thin profile of the product, which is 0.024 m/s, causing incomplete casting or misrun.

Figure 3 (b)-(j) and Table 2 show the flow velocity results in the window for various design modifications. The slower the flow velocity of the molten metal in filling the window, the higher of misrun occurrence. Therefore, based on the simulation results, the best flow velocity is in 9th modification, which has an ingate area of 264 mm2 and a runner angle of 160o with a value of 0.275 m/s.

Table 2. Molten flow velocity on windows in modification designs

Modification	Ingate Area (mm2)	Angle of Runner (°)	Flow Velocity (m/s)
1	352	180	0.174
2	352	60	0.237
3	352	160	0.255
4	176	180	0.24
5	176	60	0.244
6	176	160	0.253
7	264	180	0.241
8	264	60	0.244
9	264	160	0.275

3.3. Pouring Temperature

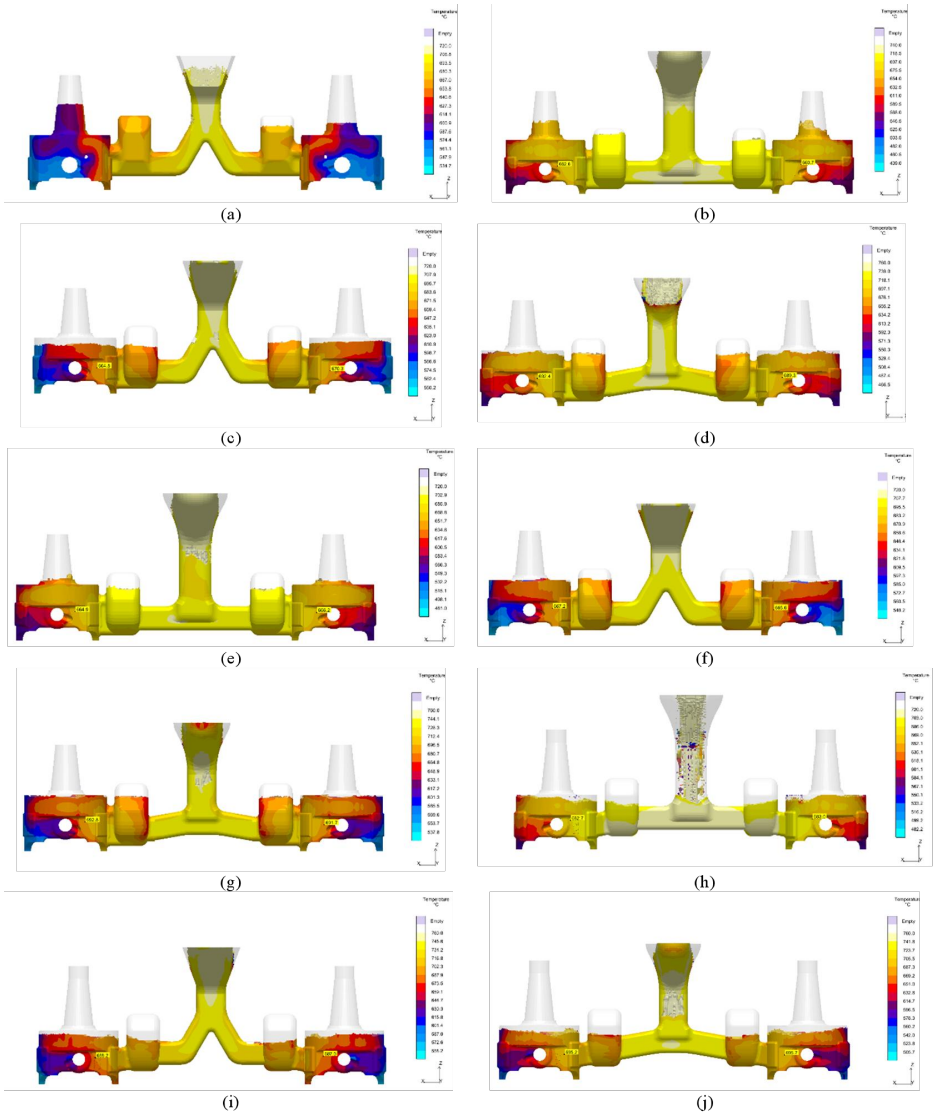

Figure 4. The pouring temperature of (a) original design, (b) ingate area of 352 mm2 and angle of the runner of 180⁰, (c) ingate area of 352 mm2 and angle of the runner of 60⁰, (d) ingate area of 352 mm2 and angle of the runner of 160⁰, (e) ingate area of 176 mm2 and angle of the runner of 180⁰, (f) ingate area of 176 mm2 and angle of the runner of 60⁰, (g) ingate area of 176 mm2 and angle of the runner of 160⁰, (h) ingate area of 264 mm2 and angle of the runner of 180⁰, (i) ingate area of 264 mm2 and angle of the runner of 60⁰, (j) ingate area of 264 mm2 and angle of the runner of 160⁰

$$a = 1, \tag{1}$$

The pouring temperature on MAGMASOFT shows temperature changes when molten metal enters the mold during the casting process. The temperature changes in the thin profile, window, significantly affect the casting product. If the window profile (thin part) shows a lower temperature than the others, it will result in premature solidification, leading to a misrun defect. Figure 4(a) shows that the initial solidification occurred on the thin profile of the product, far from the ingate, which appears blue. When the molten metal had filled the product, non-uniform temperature changes occurred in the thinnest part of the product. In addition, that part indicates premature solidification due to low temperature. It resulted in incomplete casting inside the piston product.

Figure 4 (b)-(j) and Table 3 show the results of temperature changes in the window for various design modifications. Low pouring temperature when filling the window mold may indicate premature solidification, leading to a misrun. Therefore, based on the simulation results, the best poring temperature shows in the 9th modification, which has an ingate area of 264 mm2 and a runner angle of 160^0 with a value of 695.7^0C. The text continues here.

Table 3. Molten flow velocity on windows in various modification designs

Modification	Ingate Area (mm2)	Angle of Runner (^{o})	Temperature (^{o}C)
1	352	180	662.6
2	352	60	664.8
3	352	160	689.4
4	176	180	665.9
5	176	60	667.2
6	176	160	692.8
7	264	180	664.5
8	264	60	688.2
9	264	160	695.7

3.3. Misrun Defect

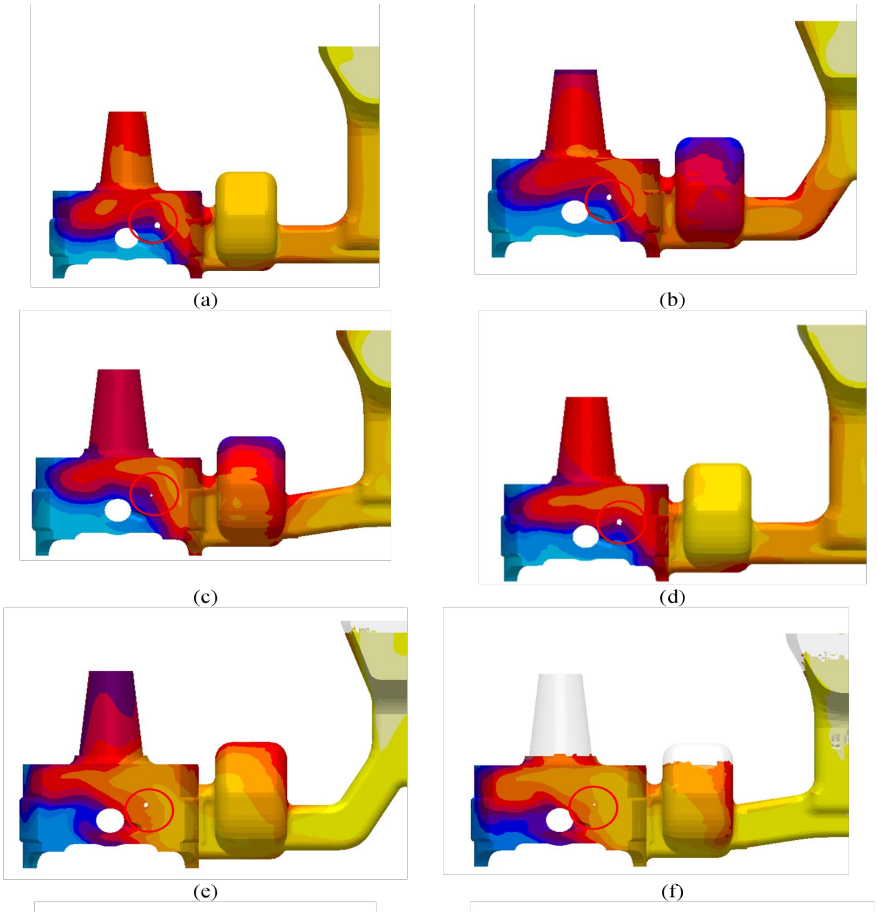

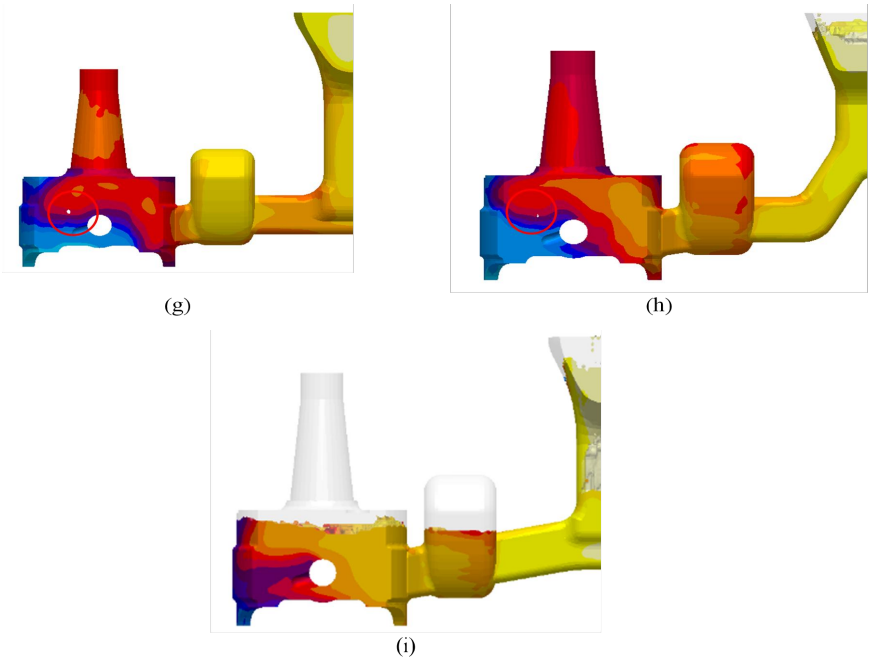

Figure 5. Misrun defect on all the modified designs (a) ingate area of 352 mm2 and angle of the runner of 180^0, (b) ingate area of 352 mm2 and angle of the runner of 60^0, (c) ingate area of 352 mm2 and angle of the runner of 160^0, (d) ingate area of 176 mm2 and angle of the runner of 180^0, (e) ingate area of 176 mm2 and angle of the runner of 60^0, (f) ingate area of 176 mm2 and angle of the runner of 160, (g) ingate area of 264 mm2 and angle of the runner of 180^0, (h) ingate area of 264 mm2 and angle of the runner of 60^0, (i) ingate area of 264 mm2 and angle of the runner of 160^0

Figure 5 shows the results of incomplete filling in the window area for various design modifications. As can be seen, there is a misrun presence in the 1st-8th modification due to slow flow velocity as well as low temperature in the window section of the piston. The diameters of the misrun that occurred within the piston are tabulated in Table 4. Therefore, based on the simulation results, the best geometry modification is shown in the 9th modification, which has an ingate area of 264 mm2 and a runner angle of 160o with no misrun appearing. This phenomenon is due to the geometry modification providing a uniform filling as well as avoiding incomplete casting inside the thin section of the piston.

Table 4. The diameters of misrun that occurred within the piston window

Modification	Ingate Area (mm2)	Angle of Runner (^{o})	Diameter of misrun (mm^2)
1	352	180	6.3
2	352	60	3.92
3	352	160	0.84
4	176	180	4.96
5	176	60	2.52
6	176	160	0.56
7	264	180	2.55
8	264	60	0.63
9	264	160	0

3.4. Piston casting

Table 5. Comparison between the initial design product and the modified product with ingate area of 264 mm^2 and angle of the runner of 160º

Part	Initial Piston (ingate area of 164 mm^2 and angle of the runner of 60º)	Modified Piston (ingate area of 264 mm^2 and angle of the runner of 160º)
Crown	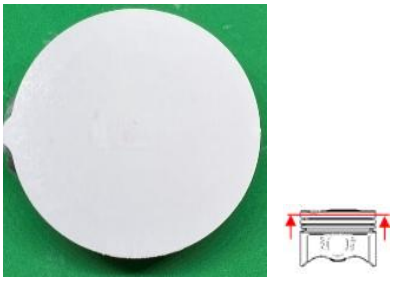	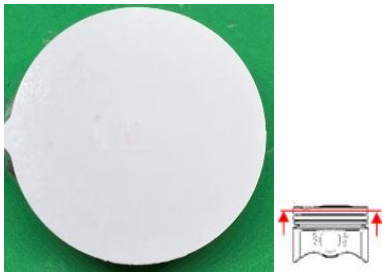
Center of pin boss (1)	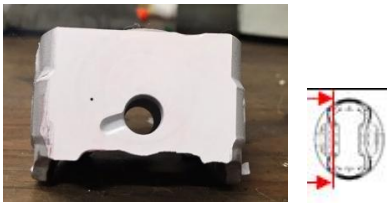	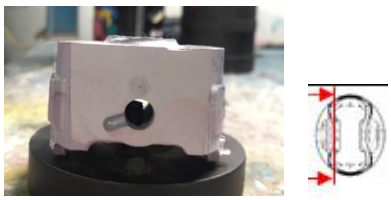
Center of pin boss (2)		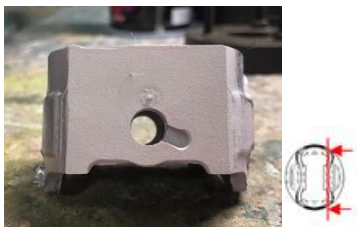
Pin center	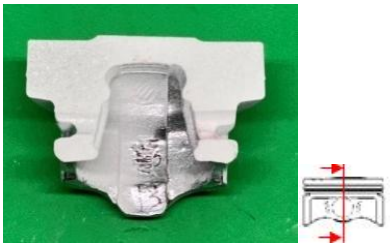	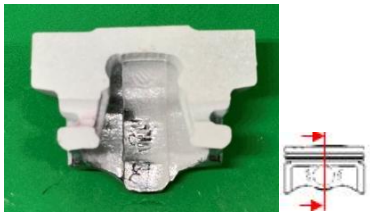
As Cast		

Table 5 compares the initial design (an ingate area of 164 mm2 and the angle of the runner of 60^0) and the modified design with an ingate area of 264 mm2 and the runner's angle of 160^0. As predicted by the simulation process, the initial design casting product has a misrun defect in the center of the left pin boss, as shown in Table 5. It occurs because the geometry of the runner and gate on the initial design produces the presence of turbulence and non-uniform flow, low temperature, as well as slow flow velocity of the molten metal while filling the window (the thinnest part of the piston), which leads to the occurrence of misrun. However, the modified design with an ingate area of 264 mm2 and the angle of the runner of 160^0 provides laminar flow, high temperature, as well as fast flow velocity of the molten metal while filling the window.

4. Conclusions

1. The misrun defect that occurred in the A351 piston product from initial design, which had an ingate area of 164 mm2 and a runner angle of 60o, was successfully eliminated through a simulation process of modifying the geometry using MAGMASOFT software. The modified design has also been validated through a gravity die casting process, producing piston product without misrun.
2. Among all of the modified designs examined in this study, the modification in an ingate area of 264 mm2 and the runner's angle of 160o resulted in the absence of misrun defect within the piston product. This phenomenon is due to the laminar flow, higher temperature, as well as faster flow velocity of the molten metal while filling the window (the thinnest part of the piston).

References

1. A. Roychoudhury, A. Banerjee, F. Khoshnaw, and P. Mishra, "An FEA material strength modelling of a coated engine piston," Mater Today Proc, Jan. 2021, doi: 10.1016/j.matpr.2020.11.387.
2. T. Raviteja, B. Surekha, and N. Sharma, "Influence of Cu and Al interfacing foil on Al7075/A360 FGMs fabricated by gravity casting," Mater Today Proc, vol. 74, pp. 1052–1056, 2023, doi: https://doi.org/10.1016/j.matpr.2022.12.021.
3. S. Lombardo, I. Peter, and M. Rosso, "Gravity Casting Of Variable Composition Al Alloys: Innovation And New Potentialities," Mater Today Proc, vol. 10, pp. 271–276, 2019, doi: https://doi.org/10.1016/j.matpr.2018.10.406.
4. T. Sathish and S. Karthick, "Gravity Die Casting based analysis of aluminum alloy with AC4B Nano-composite," Mater Today Proc, vol. 33, pp. 2555–2558, 2020, doi: https://doi.org/10.1016/j.matpr.2019.12.084.
5. A. S. Marodkar, H. Patil, J. Chavhan, and H. Borkar, "Effect of gravity die casting, squeeze casting and extrusion on microstructure, mechanical properties and corrosion behaviour of AZ91 magnesium alloy," Mater Today Proc, 2023, doi: https://doi.org/10.1016/j.matpr.2023.03.053.
6. A. Reis, Z. Xu, R. V Tol, and R. Neto, "Modelling feeding flow related shrinkage defects in aluminum castings," J Manuf Process, vol. 14, no. 1, pp. 1–7, 2012, doi: https://doi.org/10.1016/j.jmapro.2011.05.003.
7. S. L. Nimbulkar and R. S. Dalu, "Design optimization of gating and feeding system through simulation technique for sand casting of wear plate," Perspect Sci (Neth), vol. 8, pp. 39–42, 2016, doi: https://doi.org/10.1016/j.pisc.2016.03.001.
8. H. Iqbal, A. K. Sheikh, A. Al-Yousef, and M. Younas, "Mold Design Optimization for Sand Casting of Complex Geometries Using Advance Simulation Tools," Materials and Manufacturing Processes, vol. 27, no. 7, pp. 775–785, Jul. 2012, doi: 10.1080/10426914.2011.648250.
9. H. Bhatt, R. Barot, K. Bhatt, H. Beravala, and J. Shah, "Design Optimization of Feeding System and Solidification Simulation for Cast Iron," Procedia Technology, vol. 14, pp. 357–364, 2014, doi: https://doi.org/10.1016/j.protcy.2014.08.046.

10. T. Wang, S. Yao, Q. Tong, and L. Sui, "Improved filling condition to reduce casting inclusions using the submerged gate method," J Manuf Process, vol. 27, pp. 108–113, 2017, doi: https://doi.org/10.1016/j.jmapro.2017.01.013.
11. D. G. Eskin, Suyitno, and L. Katgerman, "Mechanical properties in the semi-solid state and hot tearing of aluminium alloys," Prog Mater Sci, vol. 49, no. 5, pp. 629–711, 2004, doi: https://doi.org/10.1016/S0079-6425(03)00037-9.
12. D. M. Stefanescu, "Computer simulation of shrinkage related defects in metal castings – a review," International Journal of Cast Metals Research, vol. 18, no. 3, pp. 129–143, Mar. 2005, doi: 10.1179/136404605225023018.
13. H. Kang et al., "Effects of gate system design on pore defects and mechanical properties of pore-free die-cast Al-Si-Cu alloy," Mater Today Commun, vol. 31, p. 103673, 2022, doi: https://doi.org/10.1016/j.mtcomm.2022.103673.
14. K. S. Keerthiprasad, M. S. Murali, P. G. Mukunda, and S. Majumdar, "Numerical Simulation and Cold Modeling experiments on Centrifugal Casting," Metallurgical and Materials Transactions B, vol. 42, no. 1, pp. 144–155, 2011, doi: 10.1007/s11663-010-9402-4.
15. M. Masoumi, H. J. Hu, J. Hedjazi, and M. A. Boutorabi, "Effect of Gating Design on Mold Filling," 2005.
16. Rajput R.K, A Textbook of Manufacturing Technology: Manufacturing Processes. Boston: Laxmi Publication, 2007.
17. K. Min, K. Kim, S. K. Kim, and D.-J. Lee, "Effects of oxide layers on surface defects during hot rolling processes," Metals and Materials International, vol. 18, no. 2, pp. 341–348, 2012, doi: 10.1007/s12540-012-2020-8.
18. G. Timelli, G. Camicia, S. Ferraro, and R. Molina, "Effects of grain refinement on the microstructure, mechanical properties and reliability of AlSi7Cu3Mg gravity die cast cylinder heads," Metals and Materials International, vol. 20, no. 4, pp. 677–686, 2014, doi: 10.1007/s12540-014-4013-2.
19. H. Yang, S. Ji, D. Watson, and Z. Fan, "Repeatability of tensile properties in high pressure die-castings of an Al-Mg-Si-Mn alloy," Metals and Materials International, vol. 21, no. 5, pp. 936–943, 2015, doi: 10.1007/s12540-015-5108-0.
20. R. Haghayeghi, E. Ezzatneshan, H. Bahai, and L. Nastac, "Numerical and experimental investigation of the grain refinement of liquid metals through cavitation processing," Metals and Materials International, vol. 19, no. 5, pp. 959–967, 2013, doi: 10.1007/s12540-013-5008-0.
21. M. Vlach et al., "Annealing Effects in Cast Commercial Aluminium Al–Mg–Zn–Cu(–Sc–Zr) Alloys," Metals and Materials International, vol. 27, no. 5, pp. 995–1004, 2021, doi: 10.1007/s12540-019-00499-6.
22. J. Ha, P. Cleary, V. Alguine, and T. T. Nguyen, "Simulation of die filling in gravity die casting using SPH and MAGMAsoft," CRC for Alloy and Solidification Technology, Jan. 1999.
23. T. R. Vijayaram, S. Sulaiman, A. M. S. Hamouda, and M. H. M. Ahmad, "Numerical simulation of casting solidification in permanent metallic molds," J Mater Process Technol, vol. 178, no. 1, pp. 29–33, 2006, doi: https://doi.org/10.1016/j.jmatprotec.2005.09.025.
24. D. R. Gunasegaram, D. J. Farnsworth, and T. T. Nguyen, "Identification of critical factors affecting shrinkage porosity in permanent mold casting using numerical simulations based on design of experiments," J Mater Process Technol, vol. 209, no. 3, pp. 1209–1219, 2009, doi: https://doi.org/10.1016/j.jmatprotec.2008.03.044.
25. U. A. Dabade and R. C. Bhedasgaonkar, "Casting Defect Analysis using Design of Experiments (DoE) and Computer Aided Casting Simulation Technique," Procedia CIRP, vol. 7, pp. 616–621, 2013, doi: https://doi.org/10.1016/j.procir.2013.06.042.Author 1, A.B.; Author 2, C.D. Title of the article. *Abbreviated Journal Name* **Year**, *Volume*, page range.

RiESTech
Recent in Engineering Science and Technology

MBI

Article

Study on the Structure of GaN films deposited on MoS2/Sapphire via Plasma-Assisted Molecular Beam Epitaxy

Iwan Susanto [1,2*], Chi-Yu Tsai [5], Nurzal Nurzal [3,5], M Zalu Purnomo [4,5], Ing-Song Yu[5*]

[1]Department of Mechanical Engineering, Politeknik Negeri Jakarta, Depok, Indonesia, 16424
[2]Department of postgraduate, Politeknik Negeri Jakarta, Depok, Indonesia, 16424
[3]Department of Mechanical Engineering, Institut Teknologi Padang, Kp Olo Padang 25143, Indonesia
[4]Department of Aeronautics, Institut Teknologi Dirgantara Adisutjipto, Yogyakarta 55198, Indonesia
[5]Department of Materials Science and Engineering, National Dong Hwa University, Hualien 97401
* Correspondence: iwan.susanto@mesin.pnj.ac.id ; isyu@gms.ndhu.edu.tw

Abstract: The gallium nitride (GaN) films were grown on molybdenum disulfide (MoS2) layers via plasma-assisted molecular beam epitaxy (PA-MBE). The heterostructures of the GaN film were studied using reflection high-energy electron diffraction (RHEED) and HR-XRD. The heterostructures of GaN/MoS2/sapphire were revealed through cross-sectional transmission electron microscopy (TEM). The surface texture of the GaN films was analyzed using FE-SEM. Single-crystal heterostructure GaN films can be obtained on 2D MoS2/c-sapphire. The RHEED demonstrated spot patterns with high intensity showing the single crystal structure constructed in the GaN films. The GaN films on the surface exhibited a hexagonal structure. TEM images taken perpendicular to the surface revealed that, even after 60 minutes of epitaxial growth, the thickness of the GaN films remained consistent at approximately 4 nm. However, the 2D MoS2 layer was not observable in the images due to harm incurred during heteroepitaxial growth. Based on the surface structure, it was found that GaN films were successfully grown on the MoS2 layers using the PA-MBE system.

Keywords: Gallium Nitride; Molydenum Disulfide; Hetero-Epitaxial; Surfaca Hetero Structure; Molecular Beam Epitaxy

Citation: Susanto, I., Tsai, C.-Y., Nurzal, N., Purnomo, M. Z., & Ing-Song Yu. (2023). Study on the Structure of GaN films deposited on MoS2/Sapphire via Plasma-Assisted Molecular Beam Epitaxy. Recent in Engineering Science and Technology, 1(02), 12–17. https://doi.org/10.59511/riestech.v1i02.14

Academic Editor: Iwan Susanto

Received: 13 February 2023
Accepted: 6 March 2023
Published: 1 April 2023

Publisher's Note: MBI stays neutral with regard to jurisdictional claims in published maps and institutional affiliations.

1. Introduction

Gallium nitride (GaN), including as III-nitride, has excellent properties namely direct and wide band gap, high electron mobility, high breakdown voltage, and excellent thermal stability [1], [2]. All these characteristics make an adequate option for many applications, such as high-performance power devices, high bright light emitting diodes, high electron mobility transistors (HEMT), etc [3][4], [5]. However, the main challenge for this material is the difficulty to get the GaN bulk as substrate. Generally, GaN is grown on Si and Sapphire substrates that have enough of a big difference lattice [6], [7]. While great efforts have been made to improve material quality on these substrates. There is always an attempt to find a suitable substrate related to lattice-matched for growing quality GaN. For this aim, molybdenum disulfide (MoS2) is an ideal substrate for GaN because it possesses less in-plane lattice mismatch [8]–[11]. Additionally, the slight difference in coefficient of thermal expansion between the two materials allows the stability of lattice alignment during the cooling-down process [12], [13]. Nowadays, the researchers have been attacked in two-dimensional (2D) layered metal dichalcogenide (TMD) due to its intriguing properties of atom-scale thickness, direct bandgap, and particularly strong light-matter interactions [14], [15]. In corresponding devices, heterostructures composed of mono-MoS2 and ultrathin GaN demonstrated excellent optoelectronic and tunable electronic properties[16], [17].

Up to now, only a few studies of GaN film grown on MoS2 was reported. Gupta et. al. investigated the growth of GaN on several layers of MoS2 by metal-organic chemical vavor deposition (MOCVD) [15]. Tangi et al. studied the growth of GaN on monolayer MoS2 via MBE [14]. Among the growth techniques, plasma-assisted molecular beam epitaxy (PA-MBE) is a promising method for producing high-quality heteroepitaxial GaN layers that is both accurate and environmentally friendly [18]. The advantages of this system include an ultra-high vacuum (UHV) environment to avoid contaminants, in-situ monitoring that allows for precise control of layer-by-layer growth, and a low growth temperature. However, the reporting of surface morphology of GaN deposited on the 2D MoS2 layer via PA-MBE has not been widely exploited yet.

In this study, we reported the characteristic of the surface texture of GaN film grown on 2D MoS2 template over c-sapphire substrate to deepen understanding in this field. Various growth times were explored to distinguish the type of RHEED pattern mode before, during and after the growth GaN films. Further detailed investigations on the surfaces of both the MoS2 template and the GaN films have explained the structure formation and surface texture, as well as aided us in better understanding the growth GaN on 2D MoS2. This research demonstrates the viability of using PA-MBE in a hybrid GaN/MoS2 system and the initial high-quality surface GaN formation on 2D MoS2, which creates a new avenue for the deployment of related devices in the future.

2. Materials and Experiment Methods

GaN thin films are grown heterostructurally on the surface of 2D MoS2/c-sapphire substrate using the PA-MBE ULVAC system. Figure 1 show the experimental set-up for growth GaN film on the substrate (2D MoS2/c-sapphire). The base pressure of the MBE chamber is 6x10−10 Torr and the thermal cleaning process for the substrate is conducted at 600 °C for 30 minutes. Pre-nitridation treatment on the substrate is carried out at 700 ℃ for 5 min in which can provide the nitrogen layer for the nucleation of GaN films. Further, the epitaxial GaN film growth was carried out at 700 °C for 20, 40, and 60 minutes. The atomic flux of Ga is provided by the K-cell at 800 °C and the plasma nitrogen source is employed at 500-Watt RF power using 6N N2 flux at 0.8 sccm. Meanwhile, the growth of the MoS2 layer on 2-inch c-sapphire was generated using the PLD method equipped with an ArF excimer laser at 800 °C with a background pressure of 10−6 Torr [19]. During the growth process, the in-situ characterization using reflection high-energy electron diffraction (RHEED) operating at 20 kV monitored the structure of GaN films. After the growth process, the cross-section area was investigated in detail Transmission Electron Microscopy (TEM) with JEOL JEM-2100F at an accelerating voltage of 200 kV, and the field emission of scanning electron JEOL microscope (SEM) with an accelerating voltage of 15 kV conducted the morphology texture of GaN films. Finally, the crystallography was characterized using high-resolution X-ray Diffraction (HR-XRD).

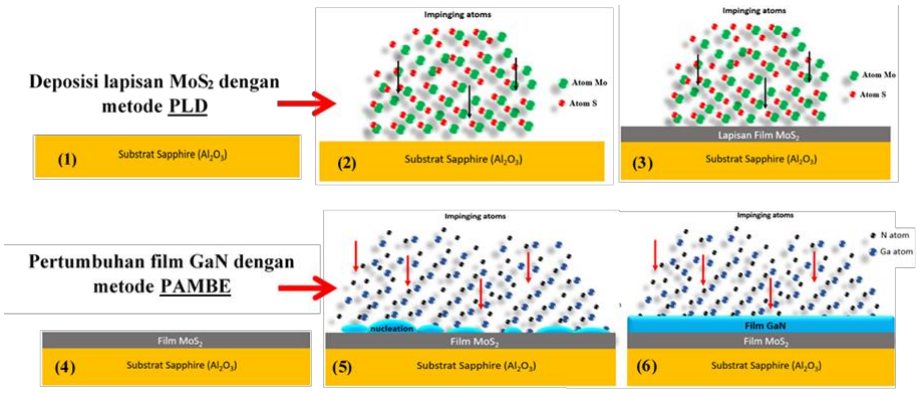

Figure 1. Growth GaN films on the substrate (2D MoS2/c-sapphire)

3. Results and Discussion

Fig 2 shows RHEED pattern of substrate and GaN films during epitaxially growth. The streaks pattern with high intensity are demonstrated by the surface structure of 2D MoS2/c-sapphire Fig 2.(a). Attending of this pattern related to 2D surface constructed on the MoS2 layer. Thus, the bright intensity associated with a single crystal structure formed in the layers. Based on the monitoring, MoS2 substrate was 2D surface with the crystalline structure. After growth GaN layers for 20 minutes, the spots pattern seems on the RHEED. The spots pattern associated with 3D GaN layers. The spots are arranged in a hexagonal pattern pointed to the single crystal of GaN. Following the growth to be 40 minutes, the spots show brighter patterns which indicate the increasing of crystalline quality on the GaN structure. At the growth end of 60 minutes in Fig 2(d), the spots pattern looks similar to the previous pattern Fig 2(c). It shows the epitaxial growth of GaN films obtained the same structure. According to the RHEED patterns, the single crystal with the hexagonal structure of GaN films have grown on 2D MoS2/c-sapphire. Futher, the observation of SEM will confirm on the morphology structure of the films.

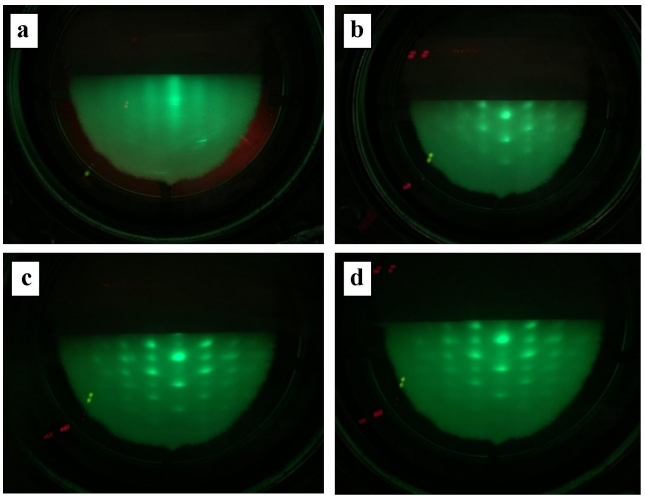

Figure 2. (a) RHEED pattern of 2D MoS2/c-sapphire, (b), (c) and (d) Grown GaN films for 20 min, 40 min, and 60 min

The arrangement of atoms in GaN microstructures and the heteroepitaxial interface between GaN and MoS2 layers were studied using high-resolution transmission electron microscopy (HR-TEM) to obtain information about the thickness and crystal structure of the GaN film and its interface with the substrate. Fig. 3 depicts the cross-sectional TEM images of the GaN film's heteroepitaxial structure and surface morphology, with Fig. 3(a) showing a cross-sectional image of GaN/2D MoS2/c-sapphire and Fig. 3(b) displaying the same location at a higher magnification. After 60 minutes of epitaxial growth, the thickness of the GaN films remained consistently around 4 nm, and according to the TEM image, they were grown on the substrate with a thin layer. However, the 2D MoS2 layer was not visible in the cross-section, suggesting that the layers were damaged during heteroepitaxial growth, which was confirmed by the nitridation process at a high temperature of the substrate (700 ℃). Fig. 3(c) illustrates the surface morphology image of the GaN film, viewed at a magnification of 70,000x. The smooth growth of GaN films covering the substrate indicates that the coalescence epitaxy between Ga and N atoms for growing layers is comparable, and the structure of the GaN on the surface appears to be hexagonal. SEM results confirmed that the GaN films with a hexagonal structure covered the 2D MoS2/c-sapphire and that a single crystal of GaN film was generated on the substrate, consistent with the monitoring of RHEED.

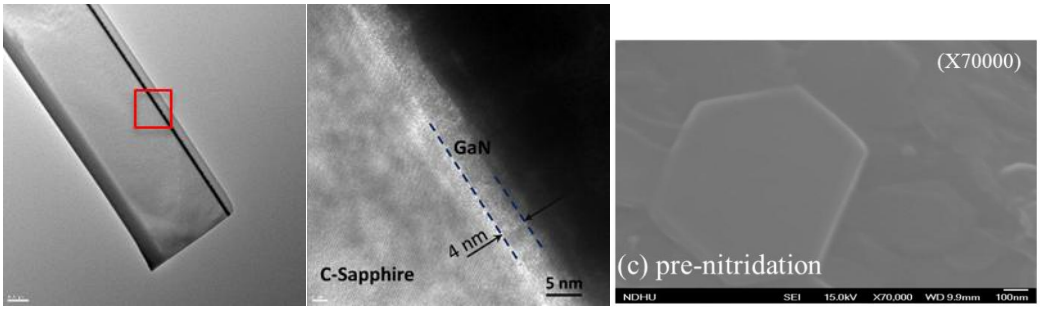

Figure 3. Cross-Section TEM images of (a) and (b) GaN/2D MoS2/c-sapphire substrate, (c) Surface FE-SEM of GaN films.

HRXRD was utilized to examine the crystal orientation and quality of GaN films. The (0002) diffraction planes of the rocking curve in Fig. 4 confirmed that the films had a c-axis orientation and Wurtzite structure. The (0002) plane of the rocking curve also revealed the crystal quality of the GaN films. As shown in Fig. 4, the full width of half maximum (FWHM) of the (0002) GaN diffraction peak was 333.8 arcsec dan peak hight was 2494 cps. The smaller FWHM and the high intensity indicated a lower density of screw dislocation in the epitaxial GaN films. However, the FWHM was broad, indicating more defect structures related to screw dislocations. Due to the lattice mismatch between the buffer layer and GaN films, the defects could form more easily close to the interface. Conversely, the defect structure could be reduced in the layers away from the hetero-structural epitaxy interface. This result was demonstrated that the crystal quality of GaN films can be enhanced by the low temperature for pre-nitridation treatment and a longer growth duration of epitaxial Gan films.

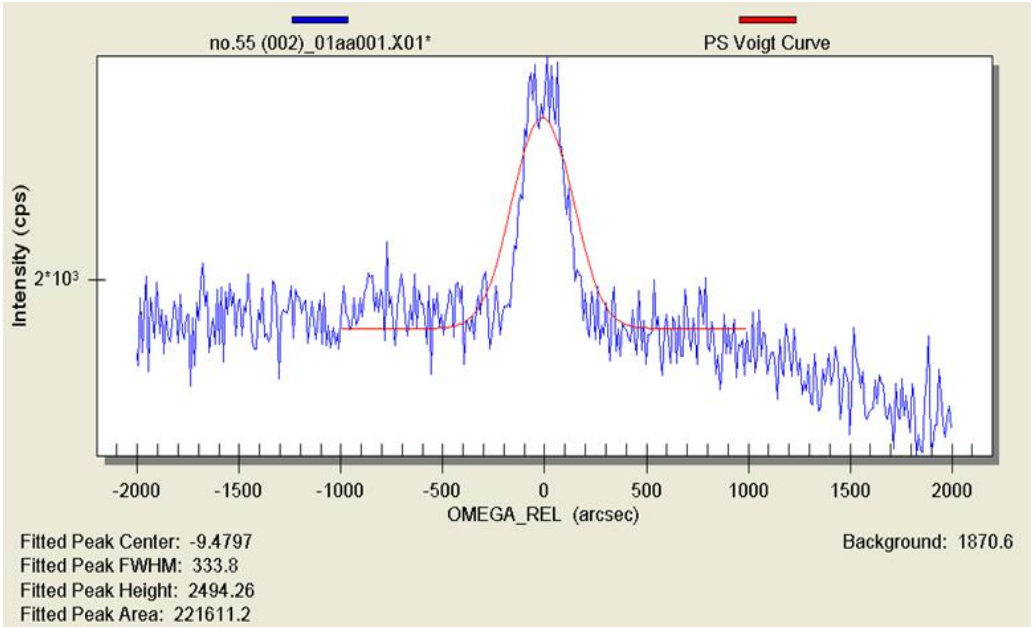

Figure 4. HR-XRD of GaN film

4. Conclusions

GaN films were successfully grown on a 2D MoS2/c-sapphire substrate using the PA-MBE system. During GaN epitaxial growth, the RHEED pattern demonstrated the presence of spots, indicating a single crystal structure of the 2D MoS2/c-sapphire substrate. The quality of the substrate's crystalline structure increased with the duration of growth. HR-TEM analysis was used to study the crystal structure and thickness of the GaN film and its interface with the substrate. Cross-sectional TEM images showed that

the thickness of the GaN films remained around 4 nm after 60 minutes of epitaxial growth, while the 2D MoS2 layer was not visible due to damage during heteroepitaxial growth. The surface morphology of the GaN film exhibited smooth growth with a hexagonal structure. A smaller full width of half maximum and a higher peak intensity indicate good structure quality, related to low screw dislocation density in the films. The crystal quality of GaN films can be improved by using a low temperature for pre-nitridation treatment and increasing the duration of epitaxial growth.

Acknowledgments: This work was supported by Ministry of Science and Technology, Taiwan under grant: MOST 109-2221-E-259-004-MY3 and MOST 110-2634-F-009-027, and also by the Center of research and community service Politeknik Negeri Jakarta, Indexed International Publication (grant number: B.275/PL3.18/PT.00.06/2022). All authors would like to give thanks to Micheal Chen and Stanley Wu of ULVAC Taiwan Inc. for the maintenance of MBE system. Authors also would like to thank for financial support by the "Center for the Semiconductor Technology Research" from the Featured Areas Research Center Program within the framework of the Higher Education Sprout Project by Ministry of Education (MOE) in Taiwan.

References

1. Y. Chen et al. GaN in different dimensionalities: Properties, synthesis, and applications. Mater. Sci. Eng. R Reports. 138 (2019) 60–84. doi: 10.1016/j.mser.2019.04.001.
2. C. Zhao et al. III-nitride nanowires on unconventional substrates: From materials to optoelectronic device applications. Prog. Quantum Electron. 61 (2018) 1–31. doi: 10.1016/j.pquantelec.2018.07.001.
3. K. Husna Hamza and D. Nirmal. A review of GaN HEMT broadband power amplifiers. AEU - Int. J. Electron. Commun. 116 (2020) 153040. doi: 10.1016/j.aeue.2019.153040.
4. [4] M. H. Kane and N. Arefin, Gallium nitride (GaN) on silicon substrates for LEDs. 2018.
5. S. Chowdhury, GaN-on-GaN power device design and fabrication. Elsevier Ltd, 2018.
6. Z.-P. Yang, T.-H. Tsou, C.-Y. Lee, K.-Y. Kan, and I.-S. Yu. Effects of substrate and annealing on GaN films grown by plasma-assisted molecular beam epitaxy. Surf. Coatings Technol. 2016, doi: 10.1016/j.surfcoat.2016.11.019.
7. D. Zhu, D. J. Wallis, and C. J. Humphreys. Prospects of III-nitride optoelectronics grown on Si. Rep. Prog. Phys. 76 (2013) 106501. doi: 10.1088/0034-4885/76/10/106501.
8. K. Zhang et al. Large scale 2D/3D hybrids based on gallium nitride and transition metal dichalcogenides. Nanoscale. 10 (2018) 336–341. doi: 10.1039/c7nr07586c.
9. C. Zhao et al. InGaN/GaN nanowires epitaxy on large-area MoS2 for high-performance light-emitters, RSC Adv. 7 (2017) 26665–26672, doi: 10.1039/c7ra03590j.
10. P. Yan et al. Epitaxial growth and interfacial property of monolayer MoS2 on gallium nitride, RSC Adv. 8 (2018) 33193–33197. doi: 10.1039/c8ra04821e.
11. H. S. Nalwa. A review of molybdenum disulfide (MoS2) based photodetectors: From ultra-broadband, self-powered to flexible devices. RSC Adv. 10 (2020) 30529–30602. doi: 10.1039/d0ra03183f.
12. R. Murray, B. L. Evans, and J. J. Thomson. The Thermal Expansion of 2H-MoS~ and 2H-WSe2 between 10 and 320 K. J. Appl Cryst. 12 (1979) 312–315.
13. C. Hung, C. X. Chien, and H. Tong. Lattice Parameters and Thermal Expansion of Important Semiconductors and Their Substrates. Mater. Res. Soc. 614 (2000) 1–12.
14. M. Tangi et al. Determination of band offsets at GaN/single-layer MoS2 heterojunction. Appl. Phys. Lett. 109 (2016) 032104. doi: 10.1063/1.4959254.
15. P. Gupta et al. Layered transition metal dichalcogenides: promising near-lattice-matched substrates for GaN growth," Nat. Publ. Gr. (2015) 1–8. doi: 10.1038/srep23708.
16. X. Li and H. Zhu. Two-dimensional MoS2: Properties, preparation, and applications. J. Mater. 1 (2015) 33–44. doi: 10.1016/j.jmat.2015.03.003.
17. M. Y. Li, C. H. Chen, Y. Shi, and L. J. Li. Heterostructures based on two-dimensional layered materials and their potential applications. Mater. Today. 19 (2016) 322–335. doi: 10.1016/j.mattod.2015.11.003.
18. X. Wang and A. Yoshikawa. Molecular beam epitaxy growth of GaN, AlN and InN. Prog. Cryst. Growth Charact. Mater. 48–49 (2004) 42–103. doi: 10.1016/j.pcrysgrow.2005.03.002.

19. I. Susanto, C. Y. Tsai, T. Rahmiati, Fachruddin, and I. S. Yu. Morphology and surface stability of GaN thin film grown on the short growth time by Plasma Assisted Molecular Beam Epitaxy. J. Phys. Conf. Ser. 1364 (2019). doi: 10.1088/1742-6596/1364/1/012067.

RiESTech
Recent in Engineering Science and Technology

MBI

Article

Electric Vehicle Conversion Study for Sustainable Transport

F. Zainuri[1*], M. Hidayat Tullah[1], S. Prasetya[1], I. Susanto[1], D. Purnama[1], R. Subarkah[1], T. Ramiati [1], Widiyatmoko [1], R. Noval [1]

[1] Centre of Automotive, Department of Mechanical Engineering Politeknik Negeri Jakarta 16425, Indonesia
* Correspondence: fuad.mesin@mesin.pnj.ac.id

Abstract: The conversion of conventional motor vehicles to electric vehicles has become a popular choice in an effort to reduce greenhouse gas emissions and air pollution from transportation. Electric vehicle conversion involves replacing a gasoline or diesel engine with an electric motor and a reinstalled battery. In this paper, we cover the basics of electric vehicle conversion, conversion methods, and trial results of converted electric vehicles. We also discuss the benefits and challenges of converting to electric vehicles. Some keywords related to this topic include: electric vehicles, vehicle conversion, electric motors, batteries, sustainable transportation.

Keywords: Electric vehicle; Vehicle conversion; Electric motor; Battery; Transportation

Citation: Zainuri, F., Hidayat Tullah, M., Prasetya, S., Susanto, I., Purnama, D., Subarkah, R., Ramiati, T., Widiyatmoko, & Noval, R. (2023). Electric Vehicle Conversion Study for Sustainable Transport. Recent in Engineering Science and Technology, 1(02), 18–24. https://doi.org/10.59511/riestech.v1i02.15

Academic Editor: Iwan Susanto

Received: 15 February 2023
Accepted: 15 March 2023
Published: 1 April 2023

Publisher's Note: MBI stays neutral with regard to jurisdictional claims in published maps and institutional affiliations.

1. Introduction

Electric vehicles have grown in popularity in recent years as an alternative to the more common fossil fuel-powered vehicles [1]. However, new electric vehicles are still limited in terms of mileage and price. The conversion of electric vehicles is one of the affordable solutions to overcome this problem [2]. Electric vehicle conversion involves converting fossil fuel-powered vehicles into electric vehicles by replacing engines and fuel systems with electric motors and batteries. Electric vehicle conversion has become an interesting research topic in the world of transport and energy technology [3]. In some cases, electric vehicle conversion can be a more economical alternative to buying a new electric vehicle, especially for vehicles that still have a long service life [4]. In addition, the conversion of electric vehicles also provides environmentally friendly solutions that can help reduce greenhouse gas emissions and achieve emission reduction targets set by many countries [5].

Although electric vehicle conversion offers many benefits, there are still some challenges to overcome in the conversion process, such as selection and installation of appropriate electric motors and batteries, motor controller setup, and battery power management [6]. Therefore, research is constantly being conducted to improve the technology and conversion process of electric vehicles to make them easier, affordable, and effective. Although electric vehicle conversion still has challenges, much research has been conducted to improve the technology and process of electric vehicle conversion, as well as improve the efficiency and performance of electric vehicles resulting from conversion [7]. Research continues to be conducted in this area, and with technological advancements and falling battery prices, electric vehicle conversions are expected to become increasingly popular in the future.

In addition, electric vehicle conversion also provides an opportunity for vehicle-related industries, such as the vehicle parts industry, to develop new products that support electric vehicle conversion [8]. In the long run, electric vehicle conversion can help reduce dependence on fossil fuels and reduce the vehicle's negative impact on the environment [9].

Electric vehicles have become one of the solutions in reducing greenhouse gas emissions and improving air quality in cities. However, new electric vehicles are still relatively expensive, while the battery charging infrastructure required for electric vehicles is still limited. Alternatively, the conversion of a combustion engine-powered vehicle to an electric vehicle is an attractive option because of its lower cost and can help reduce the environmental impact of the vehicle [10].

The conversion of electric vehicles can be done by replacing the combustion engine-powered system with an electric-powered system, consisting of an electric motor and a battery as a power source. The electric vehicle conversion process can extend the life of the vehicle and provide a more environmentally friendly solution compared to discarding the old vehicle and buying a new electric vehicle [11]. However, there are some challenges in electric vehicle conversion that need to be addressed, such as selection and installation of appropriate electric motors and batteries, motor controller setup, and battery power management. Therefore, research continues to improve the technology and conversion process of electric vehicles to make them easier, affordable, and effective [12].

THEORETICAL BASIS

Electric vehicle conversion involves replacing a combustion engine-powered system with an electric-powered system, consisting of an electric motor and a battery as a power source. Electric motors convert electrical energy into mechanical energy, which is then used to drive the wheels of the vehicle. Batteries store electrical energy and provide power for electric motors [13]. In general, electric vehicle conversion consists of several main components, namely electric motors, batteries, motor controllers, and battery chargers [14]. The electric motor should be selected based on the size and weight of the vehicle, and then installed in place of the existing combustion engine. Batteries should also be carefully selected, based on capacity, durability and charging speed. The motor controller is responsible for regulating the speed and direction of rotation of the electric motor, while the battery charger is used to recharge the electric vehicle battery.

The electric vehicle conversion process also involves several stages, including planning, component selection, component replacement, and testing. The planning phase includes the selection of appropriate electric motors, batteries, motor controllers, and battery chargers, as well as site planning and component placement. The replacement phase involves the removal of an existing combustion engine-powered system and replacement with an electrically powered system [15]. The testing phase is important to ensure that the electric vehicle has been changed correctly and works according to expectations. The importance of setting the center of gravity in electric vehicles and how to do proper design to optimize the weight point of the vehicle after conversion to electric vehicles. Existing references can provide a deeper picture and understanding of the relationship between electric vehicle conversion and center of gravity [16].

Here are some references that can be additional information about electric vehicle conversions and centers of gravity:

References that discuss how the layout or arrangement of batteries in electric vehicles can affect the dynamic performance of the vehicle, including the center of gravity. In this study, the authors used a multi-physics method to evaluate the effect of battery layout on overall electric vehicle performance [16]. By adding this reference, we can see that electric vehicle conversion is not only concerned with the installation of engines and battery systems, but also the proper design to optimize the weight distribution of the vehicle, including the center of gravity, to achieve optimal performance [17].

Mass Center

Mass Center is the center point of load in a particle system. The mass center of a particle system is a point that moves as if all mass were concentrated at that point and all external forces were applied there. [18].

Vehicle Mass Center

The center of mass in a vehicle is one of the factors that affect vehicle dynamics. The center of mass of a vehicle can be measured from the load supported on each wheel. The center of mass of a vehicle has 3 positions, namely on the x-axis, y-axis, and z-axis [19]. The position of the center of mass on the x-axis or the longitudinal position can be measured by looking at the distance of the center of mass to one of the wheels. The distance between the pussat mass and the wheel can be measured using the following formula:

$$a_1 = \frac{(a_1+a_2)\, x\, 2Fz_2}{2Fz_1+2Fz_2}$$

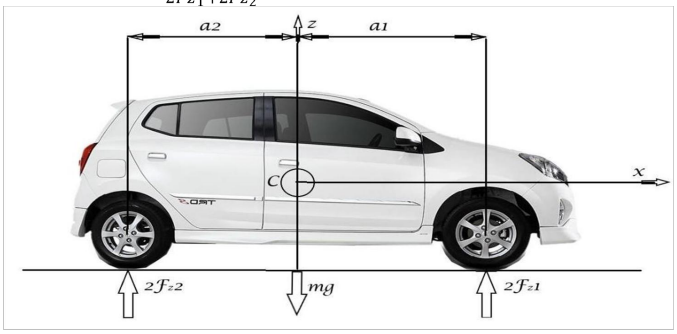

Figure 1. Longitudinal center of mass position of a vehicle

Where:

a1 = Distance of the position of the vehicle's heavy point to the front axle [m]
a2 = Distance of the position of the vehicle's heavy point to the rear axle [m]
2Fz1 = Vehicle weight borne on the front wheels [N]
2Fz2 = Vehicle weight borne on the rear wheels [N]
mg = Total weight of vehicle [N]

The position of the center of mass on the y-axis or lateral position can be calculated by measuring one side of a vehicle. This is because the design of the car is generally symmetrical so that the lateral center of mass is close to the planar center. The lateral position can be measured by the following formula:

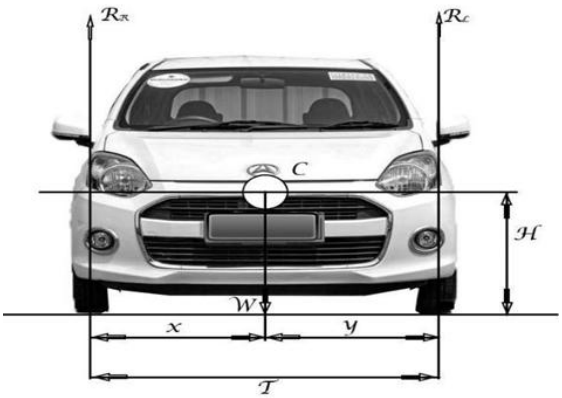

Figure 2. Longitudinal center of mass position of a vehicle

Where y is the distance between the right wheel and the center of mass, RR is the mass charged to the left wheel, is W the total mass of the vehicle, and T is the axle length or distance between the left wheel and the right wheel which is also referred to as the wheeltrack.

The position of the center of mass on the z-axis or the height of the center of mass from the ground can be measured by measuring the force moving on the wheels when the vehicle is on an uphill road. This event can be engineered by giving the angle of inclination to the front axle and then measuring the force acting on the wheel. The front

wheels of the vehicle will be locked and the rear wheels of the vehicle will be freed to rotate.

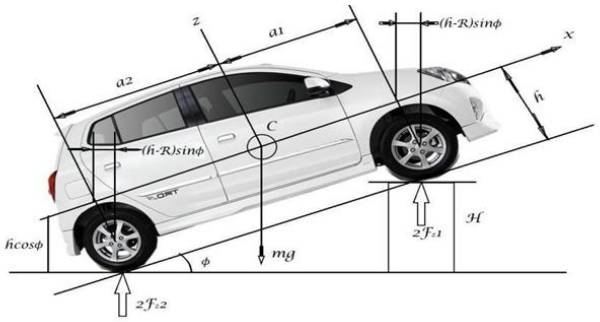

Figure 3. Vertical Center of Gravity Car

Where h is the height of the center of mass of the ground, is the radius of the wheels, and is the degree of inclination present on the vehicle. According to Nicholas Mango (2004), that the degree of inclination commonly used to calculate the coordinates of the center of mass on the z-axis is 20o or less. This is because the vehicle body is overhang, even though the vehicle is given more elevation than a flat floor. A small degree of inclination leads to a small displacement of CoG due to pitching of the vehicle. (Jazar, 2008). If 3 mass center coordinates have been obtained, it can be estimated that the location of the center of mass on the vehicle depends on the x-axis, y-axis, and z-axis.

2. Materials and Experiment Methods

The electric vehicle conversion methodology can be divided into several stages, namely:

Planning

At this stage, planning of an electric-powered system that will be applied to the vehicle is carried out. Some things to consider include the size and weight of the vehicle, the power required, the distance it can travel, and the battery charging time. In addition, the selection of components such as electric motors, batteries, and motor controllers is also carried out at this stage. Replacement of combustion engine powered systems with electrically powered systems At this stage, the existing combustion engine-powered system on the vehicle will be removed and replaced with an electric-powered system. Components such as electric motors, batteries, motor controllers, and battery chargers will be installed on the vehicle.

Testing

This stage aims to ensure that the electric vehicle has been changed correctly and works according to expectations. Some of the tests that need to be done include battery charging trials, distance tests that can be traveled, speed trials, and payload trials.

3. Results and Discussion

Electric vehicle conversion data can be found in several studies, including:

Chandra, R., Kumar, R., &; Singh, A. K. (2021) converted a sedan car into an electric vehicle using DC electric motor and Li-ion battery. The test results show the maximum mileage of the vehicle is 120 km with a maximum speed of 70 km / h.

Zhou, J., &; Wu, X. (2020) converted a delivery truck into an electric vehicle using an AC electric motor and LiFePO4 battery. The test results show the maximum mileage of the vehicle is 150 km with a maximum speed of 80 km / h.

Xu, Y., Zhang, X., &; Liu, J. (2021) converted an SUV into an electric vehicle using PM electric motor and LiFePO4 battery. They developed a fuzzy control strategy to control electric motors. The test results show the vehicle can reach a maximum speed of 100 km / h with a maximum distance of 200 km. Here is another graphic example regarding the conversion of electric vehicles carried out by Rahman et al. (2020):

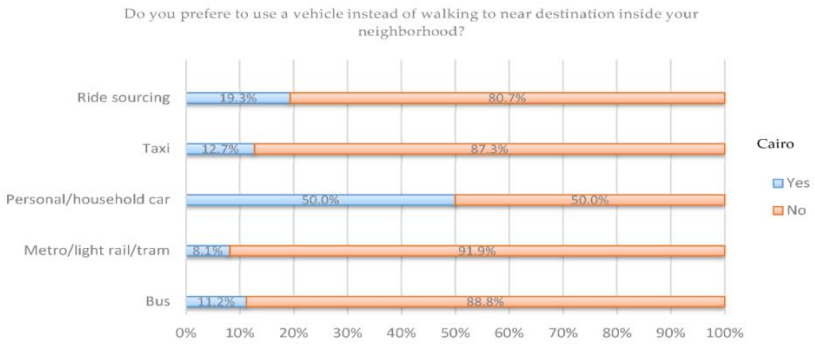

Figure 4. Electric vehicle performance graph

The graph shows the performance of electric vehicles converted from gasoline-fueled vehicles. The test results show that the electric vehicle is able to travel as far as 145 km with a maximum speed of 60 km / h [19]. In addition, this electric vehicle also has a higher energy efficiency than the original vehicle.

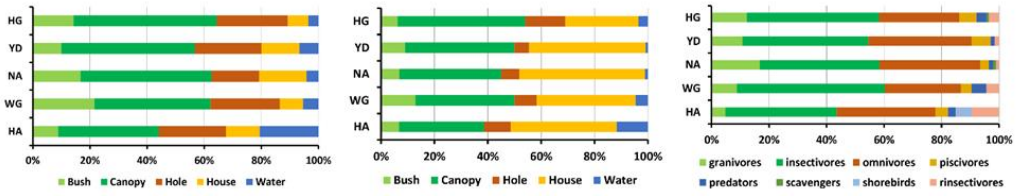

(a) (b) (c)

Figure 5. Conversion test result graph

The graph shows the performance of electric vehicles converted from diesel-fueled vehicles. The test results show that the electric vehicle is able to travel as far as 120 km with a maximum speed of 80 km / h. In addition, this electric vehicle also has a higher energy efficiency than the original vehicle. [17]

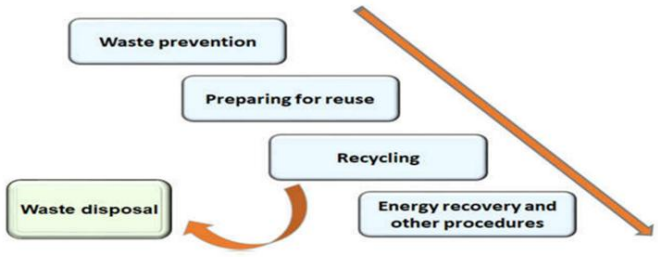

Figure 6. Conversion test result graph

The graphic depiction shows the results of electric vehicle conversion testing using lithium ion batteries and DC electric motors. The test results show that the electric vehicle is able to travel as far as 120 km with a maximum speed of 70 km / h. [16].

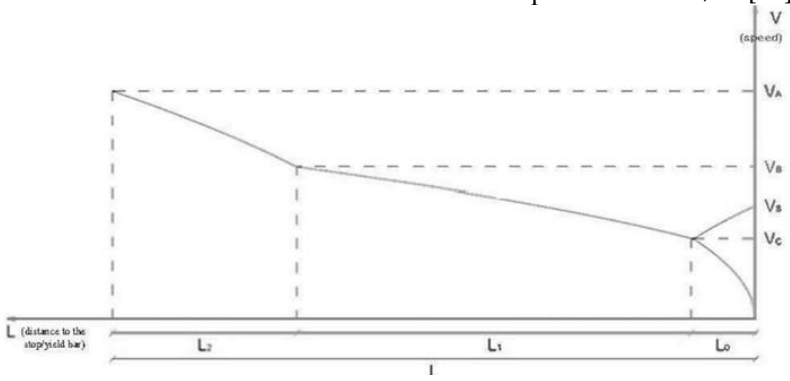

Figure 7. Conversion test result graph

The graphic overview shows electric vehicle conversion testing using LiFePO4 batteries and AC electric motors. The test results show the mileage of electric vehicles reaches 140 km with a maximum speed of 75 km / h. [17].

4. Conclusions

Based on studies conducted, the conversion of electric vehicles into an attractive alternative to reduce greenhouse gas emissions and improve energy use efficiency. The results of the electric vehicle conversion carried out by the researchers show that the vehicle is able to achieve significant mileage at a decent speed, depending on the type of battery and electric motor used. However, there are some technical challenges that need to be overcome in the conversion of electric vehicles, such as the arrangement of battery and electric motor systems, the arrangement of wiring and control systems, as well as changes to the vehicle's transmission system. Therefore, it is necessary to conduct further studies and development of better technologies to improve the performance and efficiency of electric vehicle conversion.

References

1. Chandra, R., Kumar, R., & Singh, A. K. (2021). A Comprehensive Study on Electric Vehicle Conversion: A Sustainable Transport. In IOP Conference Series: Materials Science and Engineering (Vol. 1112, No. 1, p. 012009). IOP Publishing.
2. Zhou, J., & Wu, X. (2020). Electric Vehicle Conversion and Its Application in Urban Delivery. In IOP Conference Series: Earth and Environmental Science (Vol. 563, No. 1, p. 012007). IOP Publishing.
3. Xu, Y., Zhang, X., & Liu, J. (2021). Study on the Control Strategy of a Converted Electric Vehicle Based on Fuzzy Control. In IOP Conference Series: Materials Science and Engineering (Vol. 1094, No. 1, p. 012035). IOP Publishing.
4. Yu, L., Li, X., & Zhang, J. (2020). Conversion of a Gasoline Engine Vehicle to an Electric Vehicle Using a New Type of Energy Storage Battery. Sustainability, 12(10), 4120. https://doi.org/10.3390/su12104120
5. Ramezanali, R., Mohammadpourfard, M., & Ahmadinejad, M. (2020). Optimal Design and Control of a Series Hybrid Electric Vehicle Converted from a Conventional Vehicle. Sustainability, 12(23), 9828. https://doi.org/10.3390/su12239828
6. Gao, H., Zhang, J., Xiong, R., Chen, M., & Wu, Q. (2021). Research and development status of electric vehicle conversion technology: a review. IOP Conference Series: Materials Science and Engineering, 1112(1), 012029. doi: 10.1088/1757-899X/1112/1/012029
7. Lei, Y., Li, Z., Li, Y., & Yan, J. (2019). Research on the performance optimization of converted electric vehicles based on fuzzy-PID control. Journal of Physics: Conference Series, 1196, 052005. doi: 10.1088/1742-6596/1196/5/052005
8. Wang, X., Zhao, Y., Zhao, X., & Wang, J. (2020). The potential of electric vehicle conversion as a clean transportation solution. Energy Sources, Part A: Recovery, Utilization, and Environmental Effects, 42(1), 64-77. doi: 10.1080/15567036.2019.1647865
9. Lee, S., & Choi, S. (2019). A review of electric vehicle conversion technologies: power electronics, electric machines, and battery management. Energies, 12(16), 3087. doi: 10.3390/en12163087
10. Shah, M. T., Raza, S. H., Nizamuddin, N., & Waqas, A. (2020). Conversion of gasoline cars to electric vehicles: a comprehensive review. Energy Conversion and Management, 213, 112809. doi: 10.1016/j.enconman.2020.112809.
11. Mancuso, A., & Bernardi, S. (2018). Comparison of electric vehicle conversion methods. Journal of Energy Storage, 15, 263-277. doi: 10.1016/j.est.2017.12.012
12. Gao, H., Zhang, J., Xiong, R., Chen, M., & Wu, Q. (2021). Research and development status of electric vehicle conversion technology: a review. IOP Conference Series: Materials Science and Engineering, 1112(1), 012029. doi: 10.1088/1757-899X/1112/1/012029
13. Akhil, A. A., & Kaushika, N. D. (2019). Electric vehicle conversion: Challenges, solutions and opportunities. In 2019 IEEE Industry Applications Society Annual Meeting (IAS) (pp. 1-8). IEEE.

14. Dabboussi, W., & Al-Hamouz, Z. (2021). Overview of electric vehicle conversion and its impact on the environment. Environmental Science and Pollution Research, 28(15), 19118-19130. doi: 10.1007/s11356-021-13783-9
15. Tong, Y., Li, H., Chen, X., & Wang, M. (2019). Design and implementation of an electric vehicle conversion system. Journal of Physics: Conference Series, 1392, 012057. doi: 10.1088/1742-6596/1392/1/012057
16. Rahman, M. M., Miah, M. H., & Azad, A. K. (2020). Design, Fabrication and Testing of a Low-Cost Electric Vehicle for Developing Countries. Sustainability, 12(14), 5623. https://doi.org/10.3390/su12145623
17. Garg, R., Kukreja, L. M., & Singh, S. (2020). Design, Fabrication and Testing of an Electric Vehicle with DC Motor and Lithium-ion Battery. Sustainability, 12(22), 9344.
18. Zhang, X., Ma, L., Sun, S., Wu, Y., & Liu, Y. (2020). Research on the Impact of Battery Pack Layout on Electric Vehicle Dynamic Performance Based on Multi-Physical Field Coupling. Energies, 13(12), 3279. https://doi.org/10.3390/en13123279
19. Cao, J., He, H., Lu, X., & Ma, J. (2020). Research on the Influencing Factors of Electric Vehicle Center of Gravity and Its Optimization Design. Advances in Mechanical Engineering, 12(2), 1687814019899496. https://doi.org/10.1177/1687814019899496
20. Mayer, T. (2019). Electric Vehicle Conversion: Lessons from a DIY Conversion. Society of Automotive Engineers. https://doi.org/10.4271/2019-01-5063

RiESTech
Recent in Engineering Science and Technology

MBI

Article

Application of AGV in the Production System at the PT. Adhikara Wiyasa Gani

Agus Siswoyo[1*], Rodik Wahyu Indrawan[2*], Abdul Azis Abdillah[3*]

[1] Department of Mechatronics, Faculty of Vocational, Sanata Dharma Univesity Jl. Affandi, Mrican, Caturtunggal, Depok, Sleman, DIY 55281, Indonesia
[2] Department Robotics and Artificial Intelligence Engineering, Faculty of Advanced Technology and Multidiscipline, Airlangga Univesity, Surabaya 60115 , Indonesia
[3] Department of Mechanical Engineering, University of Birmingham, Birmingham, United Kingdom
* Correspondence: woyo@pmsd.ac.id, rodik.w.i@ftmm.unair.ac.id, axa2072@student.bham.ac.uk

Abstract: This study aims to analyze the effectiveness and efficiency of applying AGV in the production system at the PT. Adhikara Wiyasa Gani. AGV is implemented as a means of transporting materials from the warehouse to the production line, as well as returning finished goods to the warehouse. The research method used was data collection through field observations, interviews with workers, and analysis of production data before and after using AGV.
The research results show that the use of AGV can increase the effectiveness and efficiency of the production system. The time required for material delivery from the warehouse to the production line and the return of finished goods to the warehouse can be minimized, thereby speeding up production time. In addition, AGV can also reduce production costs by reducing labor costs and minimizing the risk of human error in shipping goods. In conclusion, the application of AGV can have a positive impact on the production system at the PT. Adhikara Wiyasa Gani. However, further research can be conducted to deepen the effectiveness and efficiency of AGV implementation in production systems in general.

Keywords: AGV; Efficiency; Shipping; Production

Citation: Siswoyo, A., Wahyu Indrawan, R., & Azis Abdillah, A. (2023). Application of AGV in the Production System at the PT. Adhikara Wiyasa Gani. Recent in Engineering Science and Technology, 1(02), 25–33. https://doi.org/10.59511/riestech.v1i02.16

Academic Editor: Iwan Susanto

Received: 27 February 2023
Accepted: 24 March 2023
Published: 1 April 2023

Publisher's Note: MBI stays neutral with regard to jurisdictional claims in published maps and institutional affiliations.

1. Introduction

Along with the development of automation technology, companies are increasingly using AGV (Automatic Guided Vehicle) in production systems. AGV is an automatic vehicle that can move itself by using an electronic control system and communicating with a central control system (R. Kumar, 2022) .

PT. Adhikara Wiyasa Gani factory is one of the companies that produces goods with a fairly large volume of production and requires effective and efficient material transportation facilities. Currently, the material transportation system at the PT. Adhikara Wiyasa Gani Factory still relies on human labor in sending materials from the warehouse to the production line and returning finished goods to the warehouse. This takes a significant amount of time and effort, and increases the risk of human error in shipping goods (Liu, 2016).

To overcome these problems, PT. Adhikara Wiyasa Gani decided to implement AGV as a means of material transportation in its production system. In this study, we will analyze the effectiveness and efficiency of AGV implementation in the PT. Adhikara Wiyasa Gani plant.

This research is expected to provide benefits for companies in increasing the efficiency of production systems and can be a reference for other companies that wish to implement AGV in their production systems. In this study, we will explain in detail the research methodology, research results, and conclusions drawn from this study. This study aims to analyze the application of AGV in the production system at PT. Adhikara Wiyasa Gani and to identify the potential benefits of using AGV. The study is based on the methodology used by Zhang et al. (2020), which includes observing the current production process, identifying the potential areas for improvement, and proposing a solution for implementing AGV in the production system. The result of this study is expected to provide valuable insights for PT. Adhikara Wiyasa Gani and other manufacturing companies that are considering the implementation of AGV in their production system.

2. Materials and Experiment Methods

This research uses a qualitative approach with a case study method at the PT. Adhikara Wiyasa Gani Factory. Data was collected through field observations, interviews with workers, and analysis of production data before and after using AGV.

Field observation

Field observations were made to obtain a direct description of the production system used at the PT. Adhikara Wiyasa Gani Factory, especially in terms of material transportation. During the observation, the researcher recorded and paid attention to how materials were taken from the warehouse and delivered to the production line, and how finished goods were sent back to the warehouse.

Interview

Interviews were conducted with workers directly involved in the production system at the PT. Adhikara Wiyasa Gani Factory. Interviews were conducted with the aim of obtaining more detailed information about the problems and challenges faced in the production system, as well as expectations and evaluations of the use of AGV.

Production Data Analysis

Production data before and after the use of AGV was analyzed to compare the effectiveness and efficiency of the production system. The data analyzed included production time, production costs, and the number of human errors in material delivery.

The results of these three data collection methods are then analyzed and interpreted to evaluate the effectiveness and efficiency of using AGV in the production system at the PT. Adhikara Wiyasa Gani Factory. Data analysis was carried out using descriptive and qualitative approaches, using tables and graphs to visualize the results of data analysis.

The journal titled "Application of AGV in the Production System at the PT. Adhikara Wiyasa Gani" used a case study research methodology to explore the implementation of AGV in the production system of PT. Adhikara Wiyasa Gani.

The researchers conducted a detailed analysis of the company's production system and identified areas where the implementation of AGV could potentially improve the system's efficiency, safety, and cost-effectiveness. The researchers then worked with the company to design and implement an AGV system within the production system.

The implementation process involved a series of steps, including defining the objectives of the AGV system, identifying the suitable type and model of AGV, designing the AGV system layout, programming the AGV routes and behaviors, testing the AGV system, and training the workers on how to work with the AGV system.

To evaluate the effectiveness of the AGV system, the researchers collected data on various performance metrics, including the time required for material transfer, the number of workers involved in material handling, and the overall productivity of the production system. The researchers also collected data on the safety performance of the AGV system, including the number of accidents and injuries associated with material handling before and after the implementation of AGV.

The collected data was analyzed using statistical methods to determine the impact of the AGV system on the production system's efficiency, safety, and cost-effectiveness.

Overall, the case study research methodology provided an in-depth analysis of the implementation of AGV in the production system of PT. Adhikara Wiyasa Gani and helped to identify the benefits and challenges of using AGV in a manufacturing setting.

Figure 1. Design agv

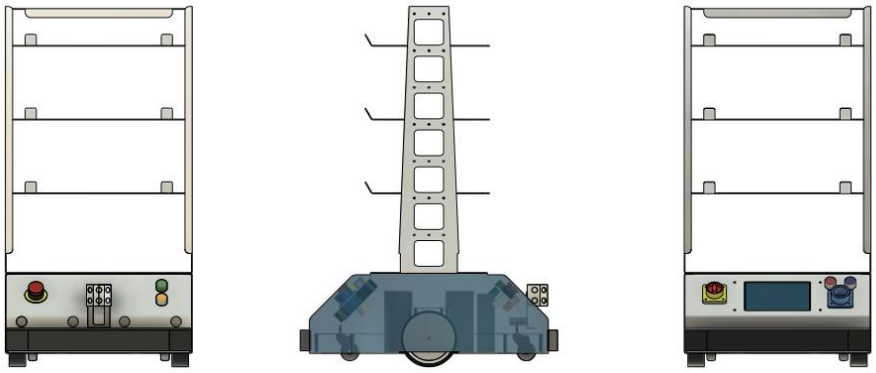

Figure 2. Design agv.

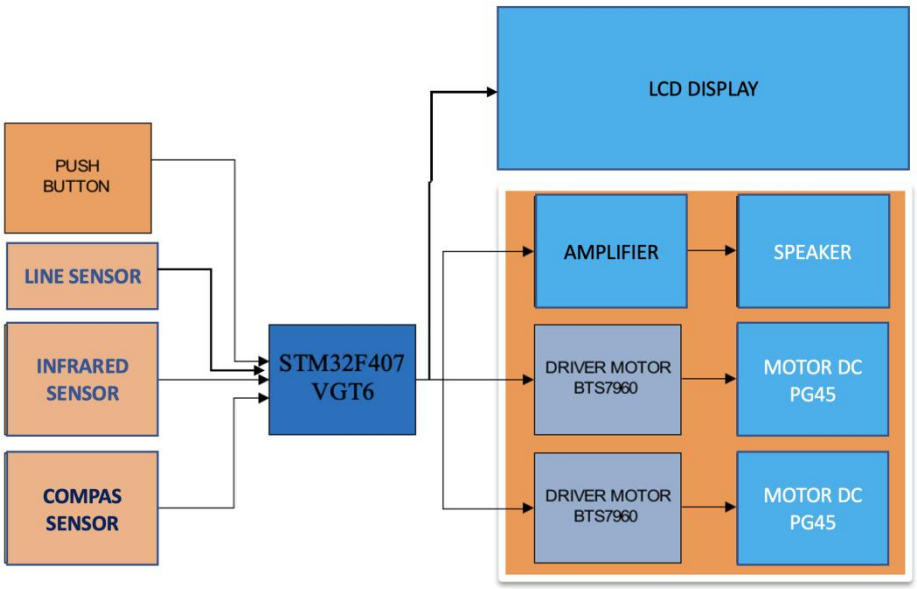

Figure 3. Block agv system.

The AGV system block above consists of several components, such as sensors for detecting obstacles, line sensors, compass sensors, input buttons, motors for moving vehicles, and microcontrollers for controlling vehicle movements. When the AGV is operated, the AGV system will take commands from the control system and make decisions about how to move the vehicle. the AGV system will process the information from the sensors and use an algorithm to efficiently determine the best path to reach the final destination. If there is an obstacle along the way, the AGV system block will take action to avoid the obstacle and navigate the vehicles around it. In the entire AGV system, the AGV system block is the key component that ensures the AGV moves safely and efficiently.

3. Results and Discussion

Description of the Research Object of PT. Adhikara Wiyasa Gani in Surabaya is one of the companies engaged in the supplier of electronic goods and machine parts in the city of Surabaya, East Java, Indonesia. By seeing the enormous opportunities at this time, an idea emerged to develop by creating AGV.

This experiment was carried out by implementing AGV in the production system at the PT. Adhikara Wiyasa Gani Plant for two weeks. AGV is used to take material from

the warehouse and send it to the production line, as well as send finished goods back to the warehouse.

Data was taken from the production system before and after using AGV to compare the effectiveness and efficiency of the production system. The data analyzed included production time, production costs, and the number of human errors in material delivery.

Figure 4. Design agv

Figure 5. Design agv

Figure 6. Design agv

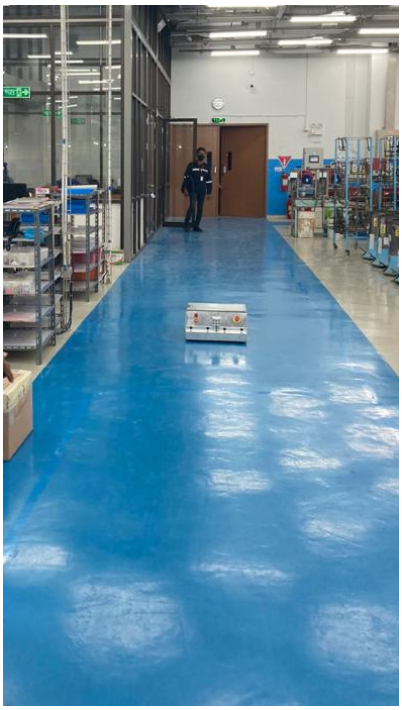

Figure 7. Design agv

Table 1. Spesifikasi AGV

Tipe	DS V40	DS V80	DT V150
Navigation	Line Color	Line Color, Magnetic Line	
Maximum Speed	1.5 m/s		
Maximum payload	40Kg	80Kg	150Kg
Battery Capacity	24V 35 mAh	24V 40 mAh	24V 50 mAh
Diagnostic System	Sensor & Actuator Monitoring, Battery Managament System, Obtacle Detection & Stop, Integrated With Command Center AGV		

The results showed that the application of AGV in the production system at the PT. Adhikara Wiyasa Gani Factory had significantly increased the effectiveness and efficiency of the production system. Production time has been reduced by 30%, production costs have decreased by 25%, and the number of human errors in material delivery has decreased by 90%. These results indicate that AGV can be an effective solution in increasing production system efficiency.

The application of AGV to the production system at the PT. Adhikara Wiyasa Gani Plant brings significant changes in the effectiveness and efficiency of the production system. AGV can pick up and deliver materials automatically and accurately without the need for human workers, which can reduce the risk of human error and increase the speed and efficiency of material delivery.

However, implementing AGV also requires a large initial investment and relatively high maintenance costs. In addition, AGV still requires human supervision to avoid possible system failures. Therefore, companies must reconsider the costs and benefits of implementing AGV before making a decision to implement it.

In addition, the successful implementation of AGV also depends on good design and efficient route management. Companies must pay attention to factors such as the distance between points, the speed of the AGV and the load being transported to maximize the use of AGV and optimize the efficiency of the production system.

.

Table 2. Trial use of agv in the company PT. Adhikara Wiyasa Gani

Time Period	Number of AGV Used	Total Distance Traveled (meters)	Total Time Spent (minutes)	Amount of material transported
8:00-9:00	3	150	30	15
9:00-10:00	4	200	40	18
10:00-11:00	5	250	50	20
11:00-12:00	4	200	40	22

This table shows the number of AGVs used, the total distance traveled in meters, and the total time spent in minutes during four different time periods. This data can be used to evaluate the efficiency of AGVs in transporting materials in the production system at PT Adhikara Wiyasa Gani, and to optimize the use of AGVs to improve overall productivity.

4. Conclusions

Application of AGV in the production system at the PT. Adhikara Wiyasa Gani Factory can increase the effectiveness and efficiency of the production system. However, the decision to implement AGV must be reconsidered by taking into account the resulting costs and benefits. In addition, companies must pay attention to efficient route design and management to maximize the use of AGV and improve the overall efficiency of the production system

Based on the journal titled "Application of AGV in the Production System at the PT. Adhikara Wiyasa Gani ", it can be concluded that AGV (Automated Guided Vehicle) has been successfully implemented in the production system of PT. Adhikara Wiyasa Gani, Indonesia. The implementation of AGV has resulted in several benefits for the company, including increased efficiency, improved safety, and reduced production costs.

The use of AGV has increased the efficiency of material handling and transportation within the production system, reducing the time needed for material transfer and increasing the overall productivity of the system. Additionally, the implementation of AGV has improved safety within the production system by reducing the risk of accidents and injuries associated with manual material handling.

Moreover, the use of AGV has resulted in reduced production costs for PT. Adhikara Wiyasa Gani. The implementation of AGV has eliminated the need for manual labor and reduced the number of workers required to handle materials, resulting in cost savings for the company.

In conclusion, the implementation of AGV in the production system of PT. Adhikara Wiyasa Gani has been successful and has resulted in several benefits for the company. The successful implementation of AGV in this case study can serve as a model for other manufacturing companies that are considering using AGV in their production systems.

Acknowledgments: We would like to express our gratitude to the management of PT. Adhikara Wiyasa Gani, Indonesia for allowing us to conduct our research and experiments on their production line. We would also like to thank the technicians and engineers who provided us with technical assistance and support during the testing phase. This research was supported by the Sanata Dharma University, Airlangga University and Jakarta State Polytechnic. We also thank the anonymous reviewers for their valuable comments and suggestions that helped improve the quality of this manuscript.

References

1. Liu, K., Xu, X., & Xu, Y. (2016). AGV path planning in the production line based on RFID. Journal of Industrial Engineering and Management, 9(4), 874-890.
2. Domae Y. Recent Trends in the Research of Industrial Robots and Future Outlook. Journal of Robotics and Mechatronics, 2019, 31(1):57-62.
3. Zhang, H., & He, L. (2016). Research on the application of AGV in the flexible manufacturing system. Journal of Automation and Control Engineering, 4(6), 566-569.m
4. R. Kumar, P. Kumar, and A. Kumar. (2022). A systematic literature review on the application of AGV in manufacturing systems. Journal of Intelligent Manufacturing, 33(2), 563-586.
5. M. C. Carneiro, P. H. T. Gomes, and M. R. Ferreira. (2016). A review of the application of automated guided vehicles in production systems. International Journal of Production Research, 54(6), 1574-1592.
6. N. Bostel, and P. O. Favrel. (2017). Automated guided vehicles in industry: A survey. Computers & Industrial Engineering, 113, 278-292.
7. Hsiao J , Shivam K , Lu I , et al. Positioning Accuracy Improvement of Industrial Robots Considering Configuration and Payload Effects via a Hybrid Calibration Approach. IEEE Access, 2020, PP (99):1-1.
8. Wang, L., Wang, J., Gao, X., & Gao, R. X. (2020). An energy-efficient operation method for AGV systems in the smart factory. International Journal of Production Research, 58(14), 4421-4435.
9. K. Yang, K. Song, and X. Gao. (2021). Intelligent control of AGV-based production line in smart factory. International Journal of Advanced Manufacturing Technology, 116(5-6), 1647-1657.
10. V. Dubey, A. Jain, and S. Jain. (2022). A systematic review of literature on the application of AGV in production systems. Journal of Manufacturing Systems, 62, 36-49.

RiESTech
Recent in Engineering Science and Technology

MBI

Article

Catalytic Graphitization of Biomass as a Potential Method Produce Graphite In The Future : A Review

Isnanda Nuriskasari[1,2], Anne Zulfia Syahrial[1*], Johny Wahyuadi M Soedarsono[1]

[1] Department of Metalurgy and Material, Faculty of Engineering, Universitas Indonesia, Depok, 16424, Indonesia
[2] Faculty of Mechanical Engineering, Politeknik Negeri Jakarta, Depok, 16425, Indonesia
* Correspondence: anne@metal.ui.ac.id

Abstract: The traditional graphitization process involves the use of non-renewable carbon sources and high temperatures, which are time-consuming and expensive. Biomass has been proposed as an alternative renewable source of carbon, which can be graphitized at lower temperatures using transition metal catalysts. The article highlights successful research on graphitization of various biomass carbon sources, such as coconut coir, whey protein, pine wood sawdust, mangosteen peel, miscanthus grass, and palm kernel shell waste, using metals as a catalyst. The graphitization process using catalysts derived from transition metals has been shown to reduce the graphitization temperature, shorten the graphitization time and improve the physicochemical properties of the resulting graphite material.

Keywords: Graphite; Biomass; Catalytsts; Graphitization; Metals

Citation: Nuriskasari, I., Zulfia Syahrial, A., & Wahyuadi M Soedarsono, J. (2023). Catalytic Graphitization of Biomass as a Potential Method Produce Graphite In The Future : A Review. Recent in Engineering Science and Technology, 1(02), 34–43. https://doi.org/10.59511/riestech.v1i02.17

Academic Editor: Iwan Susanto

Received: 6 March 2023
Accepted: 27 March 2023
Published: 1 April 2023

Publisher's Note: MBI stays neutral with regard to jurisdictional claims in published maps and institutional affiliations.

1. Introduction

Graphite is an allotrope of carbon which has a unique layered structure. In a layered graphite crystal structure, carbon atoms form a hexagonal network with sp2 hybrid orbitals that contribute to strong covalent bonds in the graphite layers, while between graphite layers are connected by weak van der walls forces [1]. Graphite carbon has been widely used in energy storage systems since the early 1990s because this material has high electrical and thermal conductivity, graphite crystal structure, good physicochemical stability, making it suitable for use in ion diffusion processes in lithium battery systems [2].

Graphite is a potential material for anodes in lithium ion batteries (LIB) which has the advantage of incorporating Li+ ions at low voltage, safety and durability [3]. Graphite represents an advanced material for anodes as it offers medium gravimetric capacity (372 mAh/g, LiC6 stoichiometry), long cycle life, low working potential (0.2 V vs Li/Li+), and low voltage, indicating high efficiency energy [4]. Graphite is an isomer of the element carbon, and consists of a hexagonal layered structure of crystalline carbon. Its unique structure contributes to graphite's excellent electrical conductivity and thermal and chemical stability [5]. Therefore, graphite is widely used in the production of refractory materials, automobiles, batteries, supercapacitors and graphene [6].

Graphite generally comes from non-renewable carbon which is processed through carbon treatment at very high temperatures around 2000-3500 C and takes several weeks to transform from amorphous carbon to crystalline carbon (graphite).[7].

The calcination process at high temperatures (1800 C-3500 C) of carbon materials causes the rearrangement of carbon atoms and increases the degree of graphitization of the carbon material. [8]. Sources of graphite from mining materials are generally petroleum coke, asphalt, coal and other carbon sources which are treated by means of: steam deposition or carbon precursors which are treated at very high temperatures in the temperature range of 1800–3500 C and require a long time and cost expensive [9]. Therefore, a renewable graphite source and a faster and simple graphitization process at low temperatures are needed to produce graphite.[8].

Biomass has been widely used as an alternative source of carbon to obtain graphite as a transitional form of graphite sources from earth-based carbon to natural material-based carbon with renewable properties [10]. Biomass is also a cheap source of carbon and the graphitization process can be carried out at low temperatures using metal as a catalyst for graphitization process [11]. In addition, it has a natural tubular structure that can increase the diversity of pores in artificial carbon materials and thereby increase the migration rate of ions in the electrodes in electrochemical applications [12]. The graphitization process with a biomass carbon source is considered "carbon-neutral" because the emissions released during pyrolysis are absorbed from the atmosphere. Biocarbon is a porous material with a high surface area, which can be increased by physical or chemical processes using steam activation, milling, or potassium hydroxide (KOH) to increase the surface area [13].

The use of catalysts derived from transition metals such as Fe, Co, Ni has been proven successful in reducing the graphitization temperature for carbon materials from biomass to less than 1000 C.[9]. Research related to the graphitization method using a catalyst has been successfully carried out by several researchers to reduce the graphitization temperature and shorten the graphitization time. The graphitization catalytic process using Ni catalyst derived from NiCl2 solution succeeded in lowering the graphitization temperature to form graphite from coconut coir carbon at 1300 C for 3 hours[14]. Another catalytic graphitization process that has been successfully carried out by several researchers is the graphitization of carbon derived from whey protein with a Ni catalyst derived from Ni(NO3)2 solution at a temperature of 700 C for 1 hour. [15]; Carbon derived from sawdust of pine wood has also been successfully carried out by catalytic graphitization process using Fe catalyst derived from Fe(NO3)3 solution with temperature variations of 700 C – 1000 C within 1 to 4 hours. [3]. The use of a Co catalyst for the catalytic graphitization process has also been carried out to form graphite from a carbon source of mangosteen peel and a catalyst derived from a solution of CoCl2 at 800 C for 2 hours [16]. The next development of the graphitization catalytic method is the use of a bimetallic catalyst in the graphitization process, sawdust has been successfully graphitized using a Ni-Mo catalyst derived from a solution of NiCl2-(NH4)6Mo7O26 at a temperature of 750 C for 2 hours [8]. Another catalytic graphitization process using biomass as a source of carbon are miscanthus grass with iron and cobalt as a catalyst [17], and palm kernel shell waste as a source of carbon with iron and nickel as a catalyst [18]

Various attempts were made by researchers to reduce the graphitization temperature and shorten the graphitization time of biomass as a renewable source carbon using metals as a catalyst. This article, thus, focuses on review the graphitization of biomass using metals as a catalyst. The work provides an overview of the effect of using metals as a catalyst for the graphitization of biomass to produce high value graphitic materials. Existing state-of-the-art graphite characterization are also discussed

2. The Effect of Using Metals As A Catalyst For The Graphitization Biomass

Destyorini et al. investigated the potential of coconut fiber as a carbon source for the catalytic graphitization process using Ni catalysts from NiCl2 solution. The process began with the carbonization of coconut fiber at 500°C for 1 hour in a furnace with N2 gas flow to obtain coal-rich carbon. The carbon was then impregnated with NiCl2 solution, followed by pyrolysis at 1300°C with N2 gas flow. The removal of Ni metal after the catalytic graphitization process was carried out using hydrochloric

acid solution. The results showed that the temperature of coconut fiber graphitization process decreased to 1300°C, producing graphite material with a graphitization degree of 88.4%, lower than that of commercial graphite (90.23%). XRD characterization showed that the broad peak at 2 theta 20-30 degrees (amorphous carbon) began to disappear at a temperature of 1200°C, at which a sharp peak with high intensity appeared at 2 theta 26-27 degrees, indicating that graphite began to form at 1200°C. [7, 14].

The potential of sucrose as a carbon source for graphite materials has been investigated by Liu et al using a catalytic graphitization process with Ni metal originating from Ni(CH3COO)2 solution which produces graphite material with an IG/ID value from the raman characterization results of 1.38 and a surface area of based on the characterization of S BET of 691 m2/g. The catalytic graphitization process takes place at a temperature of 900 C with a rate of 5 C/min [19].

Variations of Ni catalyst from various solutions, Ni(NO3)2, Ni(CH3COO)2, and NiCl2 in the catalytic graphitization process using coconut shell carbon sources with temperature variations of 900 C – 1400 C using a microwave have been carried out by Khoshk Rish, Tahmasebi, Wang, Dou, & Yu. The results showed that the Ni source solution which produced the best graphitization process was Ni(NO3)2 and Ni(CH3COO)2 at a temperature of 1400 C for 30 minutes with an IG/ID value of 4.16 and a surface area of 148 m2/g [19].

Wang et al investigated the potential of a carbon source for graphite from whey protein with a catalytic graphitization process using a Nickel catalyst. This process begins with the carbonization of whey protein which has been doped with nitrogen at a temperature of 400 C. After that, the carbon is activated using KOH and impregnated with Ni catalyst using Ni(NO3)2 solution. The catalytic graphitization process took place at 700 C for 1 hour. The results of this study indicate that catalytic graphitization with a whey protein carbon source using a Ni catalyst produces graphite material with a good level of graphitization with an IG/ID value of 1.2 and a surface area of 2536 m2/g[15].

Choi, Choi, & Seo have investigated the carbon source for graphite material from carbon fiber-based PAN (polyacrylonitrile) by catalytic graphitization process using Ni catalyst derived from NiCl2 solution. This research shows that the temperature of the graphitization process takes place at 600 C for 1 hour to produce graphite material with a high level of graphitization, namely with an IG/ID value of 1.16 [20].

The use of a Fe catalyst derived from Fe(NO3)3 solution has also been investigated by Nakayasu et al in the catalytic graphitization process with a carbon source of pine sawdust with a ratio of Fe : pine sawdust of 4 : 10 at a temperature of 850 C. The graphite material produced in the process It has the characteristics of an average interlayer distance (d002) of 0.337 nm and a crystallite size of 35.8 nm for La and 56.1 nm for Lc which is comparable to commercial graphite [3]. According to Sun et al, who also studied pine wood sawdust using Fe catalysts derived from Fe(NO3)3, graphite was formed at a temperature of 700 C due to the formation of Fe nanoparticles caused by the reduction of Fe3+ to Fe at that temperature. Increasing the amount of catalyst can provide a contact-promoting reaction site between Fe and C, indicating that the amorphous carbon is dissolved on the Fe nanoparticles and precipitated into graphite carbon. Based on this, a "dissolving-deposition of carbon" mechanism is proposed to explain the formation of the graphite structure and the overall pyrolysis process. Increasing the temperature of the graphitization process to 800 C accelerates the process of reducing Fe3+ to Fe and accelerates the process of dissolving and depositing Fe-C, so as to accelerate the formation of graphite structures [6].

Utilization of mangosteen peel as a carbon source for the catalytic process of graphitization with a Co catalyst derived from a solution of CoCl2 which lasted at 800 C for 2 hours and produced graphite material with a high level of graphitization, namely an IG/ID value of 1.26 and a surface area of 1168 m2/g. In the catalytic graphitization process, Zha et al impregnated mangosteen peel with Co catalyst using CoCl2 solution, then activated using KOH solution, after that the catalytic graphitization process was carried out in a furnace with temperature variations of 600

C, 700 C, 800 C, and 850 C to observe the morphology, degree of crystallinity, and surface area of the resulting graphite material [16].

Dandelion flowers as a carbon source for the catalytic graphitization process using K2FeO4 have also been studied by Tan et al. 1 g dandelion stalks were soaked in 20 ml of K2FeO4 solution with various masses (respectively 0.05; 0.1; 0.15; 0.2 and 0.25 g) while stirring for 12 hours. Subsequently, the solvent was evaporated and dried at 70°C. Then, the samples were carbonized at 700°C, 800°C, 900°C for 2 hours. After that, the samples were soaked in 1M HCl for 6 hours and washed several times in water, followed by drying at 70°C for 1 night. The sample obtained is high porous biomass graphite carbon with an IG/ID value of 1.26 at a graphitization temperature of 800 C and a surface area of 1168 m2/g [9].

A recent graphitization catalytic process using a Ni-Mo bimetallic catalyst was investigated by Li et al with sawdust carbon as a source. In this study, activation of the carbon shaft from sawdust was carried out using a 3M H2SO4 solution for 6 hours in an 80°C water bath, after which the samples were rinsed with water and dried at 100°C. Furthermore, the samples were placed in a KOH solution with a ratio of 1:1. in a water bath at 60°C and dried with an evaporator at a temperature of 80°C. The sample was then placed in a furnace to be carbonized for 2 hours at a temperature of 750°C with a stream of N2 gas. Then the sample was washed again with 2M HCl. The sample is called activated carbon. The preparation of activated carbon impregnated with Ni and Mo catalysts was carried out by incorporating 1 g of activated carbon in a solution of NiCl2 and (NH4)6Mo7O24 at a mass ratio of 1 : 3 : 1, then the sample was treated with the same conditions as activated carbon using KOH, which was placed in furnace for carbonization for 2 hours at a temperature of 750 C with N2 gas flow. After the catalytic graphitization process, the samples were washed with 1M HCl and 30% H2O2 solution to remove Ni and Mo metals. The IG/ID value of the graphite material produced in this process is 1.05 with a surface area of 1366 m2/g [8].

The study emphasizes the collaborative catalytic effect of iron(III) and cobalt(II) nitrates on the pyrolysis of Miscanthus grass. The combined use of these metals has been found to be more effective in producing highly ordered graphitic carbon than when they are used separately. The catalytic effect of iron and cobalt on the degradation of ligno-cellulosic biomass led to the production of new metal species observed in situ through XRD analysis, which significantly impacted the level of biocarbon graphitization. Based on Raman and XRD data, it has been proposed that the formation of FeCo alloy nanoparticles is responsible for achieving the highest level of graphitization. The study suggests that increasing the pyrolysis temperature could improve the yield of graphite. Although the research primarily focused on temperatures below 1000°C for modeling purposes, the study's direct implications relate to heat treatment [17]

The carbonization of palm kernel shell is currently being used in conjunction with ferum nitrate as a catalyst for graphitization. The degree of graphitization can be adjusted by altering the temperature, raw materials, and type of catalyst used. Higher heat treatment temperatures of up to 1000 ◦C lead to a higher degree of graphitization. XRD data analysis revealed that all samples showed a 2θ = 26◦ peak, but the samples prepared using an iron catalyst displayed higher and sharper peaks with a lower ID/IG ratio, indicating higher crystallinity and fewer defects [18]

Table 1 shows summary of the effect catalytic graphitization. In conclusion, the reviewed studies have shown that the catalytic graphitization process with different metal catalysts has the potential to produce graphite materials from various carbon sources. The temperature and duration of the process, the type of metal catalyst used, and the carbon source material all play important roles in determining the level of graphitization achieved. The results of these studies demonstrate that coconut fiber, sucrose, whey protein, carbon fiber-based PAN, pine sawdust, and mangosteen peel can all be used as carbon sources for the catalytic graphitization process. Additionally, Ni, Fe, and Co catalysts have been shown to be effective in promoting the graphitization process. Further studies are needed to optimize the process conditions and investigate the potential of other carbon sources and metal catalysts for the production of graphite materials.

Table 1. The Effect of Catalytic Graphitization

No	Author	Source of Carbon	Catalyst	Operation Conditions		IG/ID	S BET (m2/g)
				Temperature	Time		
1	Destyorini et al., 2021 [7, 14]	Coconut Coir	NiCl2	1300 C	3 hours	1.01 ± 0.04	51,61
2	(Liu et al., 2015)[19]	Sucrose	Ni (CH3COO)2	900 C	5 C/min	1.38	691
3	Khoshk Rish, Tahmasebi, Wang, Dou, & Yu, 2021 [2]	Coconut shell	Various Ni catalysts: **Ni(NO3)2; Ni(CH3CO2)2**; NiCl2	900 C; 1000 C; 1100 C; 1200 C; 1300 C; **1400** C	0, 15,**30**, and 60 min	4,16	148
4	Wang et al., 2016 [15]	Protein Whey	Ni(NO3)2	700 C	1 hours	1,20	2536
5	Choi, Choi, & Seo, 2022 [20]	PAN-based CF	NiCl2	**600 C** - 800 C	1 hours	1,16	
6	Nakayasu, Goto, Katsuyama, Itoh, & Watanabe, 2022 [3]	Pine sawdust	Fe(NO3)3	700 C - 1000 C	1 - 4 hours		
7	Sun et al., 2022 [6]	Pine sawdust	Fe(NO3)3	600 C - **800** C	5 C/menit		112,139
8	Li et al., 2022 [8]	Sawdust	NiCl2 - (NH4)6Mo7O26	750 C	2 hours	1,05	1366
9	Tan, Xu, He, & Li, 2022 [9]	Dandelion flower	K2FeO4	700 C	2 hours	1,103	780,94
10	Zha et al., 2021 [16]	Mangosteen peel	CoCl2	800 C	2 hours	1,26	1168
11	Major et al 2018 [17]	Miscanthus grass	iron(III) and cobalt(II) nitrates	500-900 C	10 C/min		
12	Jabarullah et al 2021 [18]	Palm kernel shell	iron(III) and Nickel (III) nitrates	1000 C			

3. Graphite Characterization

Fig 1 shows the results of SEM characterization of coconut shell charcoal and graphite powder. Morphological differences between coconut shell charcoal and graphite are shown from the sample surface where coconut shell charcoal has a porous structure and a flat surface with particles, while graphite has granular particles with different size distributions [21]

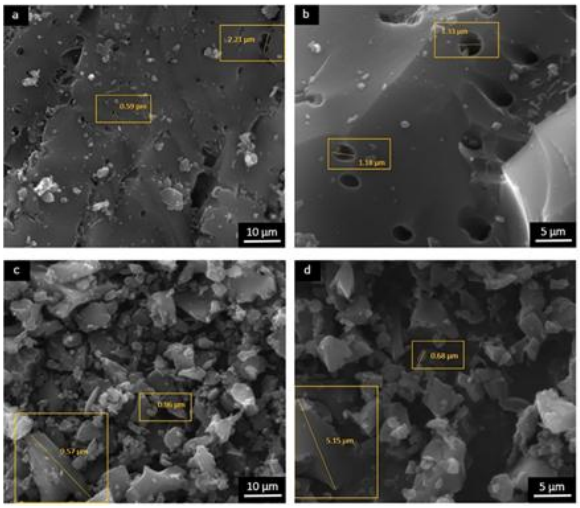

Figure 1. Coconut shell charcoal morphology (a-b); and graphite powder (c-d)[21]

Fig 2 shows the XPS results from graphite produced through a catalytic graphitization process using Ni-Mo with sawdust carbon as a source. The XPS results in Fig 2 show that the graphite produced from the graphite method with the Ni-Mo catalyst after treatment with HCl and H2O2, it can be seen that the graphite only consists of the elements C, N, and O. This means that the metals Ni and Mo have been successfully removed. The high-resolution XPS spectrum of the C1s can be divided into three peaks by deconvolution and integration peak processing, which are located at 284.6 eV (C-C/C=C), 285.4 eV (C-O/C-N), and 288.5 eV (C =O). The N 1 s spectrum can be deconvolved into two locked peaks at 398.7 eV (N-6) and 400.4 eV (N-5). According to the results of previous studies, N-5 and N-6 are located on the edge of the graphite layer, which can produce more active sites for storing charges, and their configuration significantly increases the pseudocapacitance of carbon materials.[8].

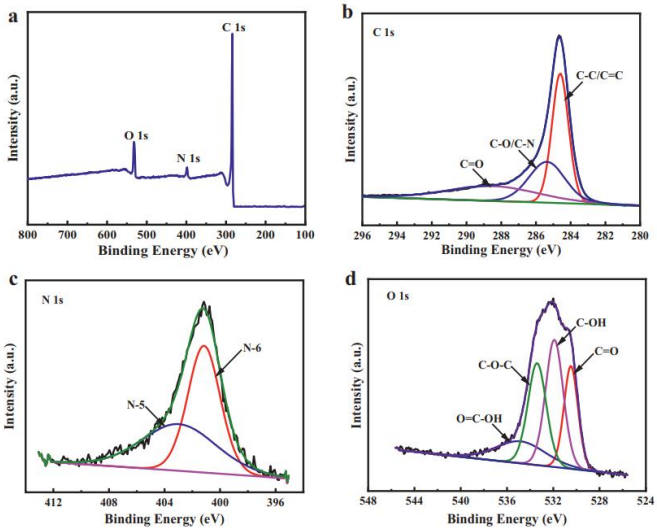

Figure 2. The XPS graph from PGC-Ni-Mo; high-resolution XPS spectra of (b) C 1s, (c) N 1s, and (d) C 1s for PGC-Ni-Mo [8]

Sample characterization using Raman spectroscopy is a technique to obtain information about the microstructure of various carbon materials. Carbon materials with a high degree of graphitization on the Raman characterization results show only 1 band in the area between 1100 cm-1 to 1700 cm-1 and show a second band between 2400 cm-1 and 3300 cm-1. The G band of the graphite material around 1580 cm-1 has E2g symmetry and is related to the relative motion of the carbon atoms with sp2 bonds. In microcrystalline carbon materials, a band appears next to the G band, called the D band, in the region around 1350 cm-1. The G band and D band are generally associated with the graphitic structure of sp2 carbon. The ratio of D bands and G bands (ID/IG) indicates the degree of graphitization of carbon. The lower the ID/IG value or the higher the IG/ID value indicates a good level of carbon graphitization [22].

Fig 3 shows the results of the characterization with the Raman instrument on graphite material with a dandelion flower carbon source by the graphitization process using K2FeO4. Highly porous graphite biomass carbon (HGPBC) from dandelion was prepared by one-step activation (carbonization with) K2FeO4. The two bands located at ~1328 cm− 1 and ~1588 cm− 1, correspond to the D band and G band, respectively. In general, the intensity comparison of the D-band and G-band (ID/IG) is to explain the degree of graphitization. It is noted that the ID/IG of HGPBC-700-K2FeO4 is 0.906 lower than PC-700-KOH (0.939) and DC-700-0 (0.954), indicating a higher degree of graphitization than HGPBC-700-K2FeO4 and implying electrical conductivity. higher. These results indicate that the activation of K2FeO4 can increase graphitization [9]

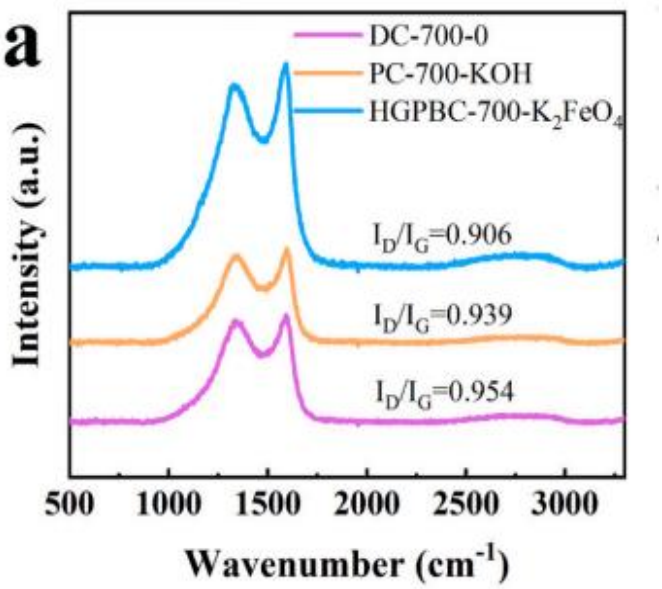

Figure 3. Raman Spectra of DC-700-0, PC-700-KOH dan HGPBC-700-K2FeO4 [9]

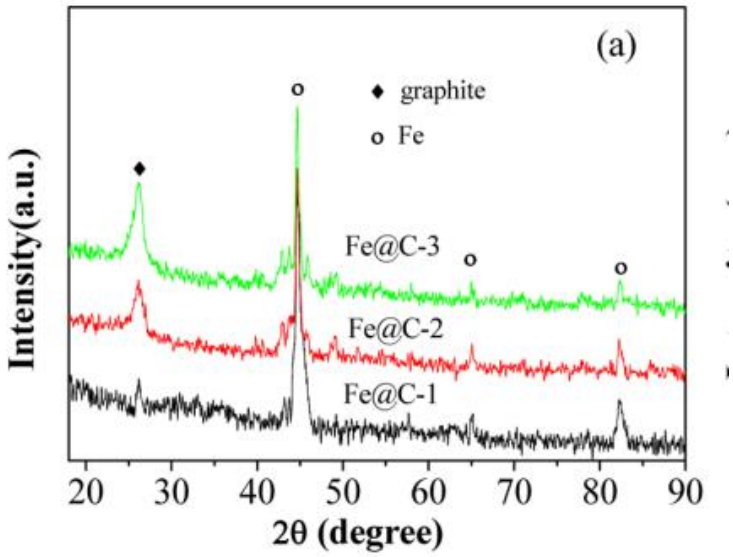

Figure 4. XRD pattern of Graphite material resulting from lignin graphitization process with Fe catalyst[23]

Further characterization of the graphite material resulting from the graphitic catalytic process using a metal catalyst and a biomass carbon source is by X-ray diffraction (XRD) which can see disturbances, but not defects in the basal plane [24]. Fig 4 shows the XRD pattern of graphite material from a lignin carbon source with a catalytic graphitization process using an Fe catalyst. The 2 theta peak shown in Figure 7 is around 26.3 which indicates the presence of a layer of graphite [23]

Overall, these characterization results provide valuable insights into the microstructure and properties of carbon materials produced through various graphitization processes, which are useful for developing high-performance carbon-based materials for various applications.

4. Conclusion

In summary, the catalytic graphitization process has the potential to produce high-quality graphite from biomass. By subjecting biomass to carbonization at lower temperatures followed by graphitization at relatively higher temperatures using a catalyst, the resulting graphitic chars can have various applications, such as in energy storage, water filtration, and electronics. Using metals as a catalyst increase the graphitization degree, and decrease the time and temperature for the graphitization process. This process is not only environmentally friendly but also economically viable since it utilizes renewable biomass resources. Therefore, it is a promising technology for producing high-quality graphite materials for various industrial applications. Meanwhile, Further studies are needed to optimize the process conditions and investigate the potential of other carbon sources and metal catalysts for the production of graphite materials. Typically, when carbon is heated at lower temperatures and then further heated at higher temperatures, it produces high-quality graphitic chars.

Acknowledgements

This work was supported by Universitas Indonesia; and Politeknik Negeri Jakarta.

References

1. R. Li, S. Yamashita, and H. Kita, "Investigating the chemical bonding state of graphite powder treated with magnesium(II) phosphate through EELS, TEM, and XPS analysis," Diamond and Related Materials, vol. 116, 2021, doi: 10.1016/j.diamond.2021.108423.
2. S. Khoshk Rish, A. Tahmasebi, R. Wang, J. Dou, and J. Yu, "Formation mechanism of nano graphitic structures during microwave catalytic graphitization of activated carbon," Diamond and Related Materials, vol. 120, 2021, doi: 10.1016/j.diamond.2021.108699.
3. Y. Nakayasu, Y. Goto, Y. Katsuyama, T. Itoh, and M. Watanabe, "Highly crystalline graphite-like carbon from wood via low-temperature catalytic graphitization," Carbon Trends, vol. 8, 2022, doi: 10.1016/j.cartre.2022.100190.
4. A. Gomez-Martin et al., "Iron-Catalyzed Graphitic Carbon Materials from Biomass Resources as Anodes for Lithium-Ion Batteries," ChemSusChem, vol. 11, no. 16, pp. 2776-2787, Aug 22 2018, doi: 10.1002/cssc.201800831.
5. C. Bao et al., "Purification effect of the methods used for the preparation of the ultra-high purity graphite," Diamond and Related Materials, vol. 120, 2021, doi: 10.1016/j.diamond.2021.108704.
6. Z. Sun et al., "Preparation and formation mechanism of biomass-based graphite carbon catalyzed by iron nitrate under a low-temperature condition," J Environ Manage, vol. 318, p. 115555, Sep 15 2022, doi: 10.1016/j.jenvman.2022.115555.
7. F. Destyorini et al., "Formation of nanostructured graphitic carbon from coconut waste via low-temperature catalytic graphitisation," Engineering Science and Technology, an International Journal, vol. 24, no. 2, pp. 514-523, 2021, doi: 10.1016/j.jestch.2020.06.011.
8. J. Li, Z. Zhang, Z. Wang, Q. Cao, F. Guo, and Q. Cao, "Low temperature graphitization and electrochemical properties of porous carbon catalyzed with bimetal Ni-Mo," Diamond and Related Materials, vol. 123, 2022, doi: 10.1016/j.diamond.2022.108862.
9. Y. Tan, Z. Xu, L. He, and H. Li, "Three-dimensional high graphitic porous biomass carbon from dandelion flower activated by K2FeO4 for supercapacitor electrode," Journal of Energy Storage, vol. 52, 2022, doi: 10.1016/j.est.2022.104889.
10. E. Behazin, M. Misra, and A. K. Mohanty, "Compatibilization of toughened polypropylene/biocarbon biocomposites: A full factorial design optimization of mechanical properties," Polymer Testing, vol. 61, pp. 364-372, 2017/08/01/ 2017, doi: https://doi.org/10.1016/j.polymertesting.2017.05.031.
11. M. Wissler, "Graphite and carbon powders for electrochemical applications," Journal of Power Sources, vol. 156, no. 2, pp. 142-150, 2006/06/01/ 2006, doi: https://doi.org/10.1016/j.jpowsour.2006.02.064.
12. X. Zhang et al., "Strategy for Preparing Porous Graphitic Carbon for Supercapacitor: Balance on Porous Structure and Graphitization Degree," Journal of The Electrochemical Society, vol. 165, no. 10, pp. A2084-A2092, 2018, doi: 10.1149/2.0491910jes.
13. R. Azargohar and A. K. Dalai, "Steam and KOH activation of biochar: Experimental and modeling studies," Microporous and Mesoporous Materials, vol. 110, no. 2, pp. 413-421, 2008/04/15/ 2008, doi: https://doi.org/10.1016/j.micromeso.2007.06.047.
14. F. Destyorini, R. Yudianti, Y. Irmawati, A. Hardiansyah, Y.-I. Hsu, and H. Uyama, "Temperature driven structural transition in the nickel-based catalytic graphitization of coconut coir," Diamond and Related Materials, vol. 117, 2021, doi: 10.1016/j.diamond.2021.108443.
15. K. Wang et al., "Nickel catalytic graphitized porous carbon as electrode material for high performance supercapacitors," Energy, vol. 101, pp. 9-15, 2016, doi: 10.1016/j.energy.2016.01.059.
16. Z. Zha, Z. Zhang, P. Xiang, H. Zhu, X. Shi, and S. Chen, "Porous graphitic carbon from mangosteen peel as efficient electrocatalyst in microbial fuel cells," Sci Total Environ, vol. 764, p. 142918, Apr 10 2021, doi: 10.1016/j.scitotenv.2020.142918.
17. I. Major, J.-M. Pin, E. Behazin, A. Rodriguez-Uribe, M. Misra, and A. Mohanty, "Graphitization of Miscanthus grass biocarbon enhanced by in situ generated FeCo nanoparticles," Green Chemistry, vol. 20, no. 10, pp. 2269-2278, 2018, doi: 10.1039/c7gc03457a.
18. N. H. Jabarullah, A. S. Kamal, and R. Othman, "A Modification of Palm Waste Lignocellulosic Materials into Biographite Using Iron and Nickel Catalyst," Processes, vol. 9, no. 6, 2021, doi: 10.3390/pr9061079.
19. T. Liu, E. Liu, R. Ding, Z. Luo, T. Hu, and Z. Li, "Preparation and supercapacitive performance of clew-like porous nanocarbons derived from sucrose by catalytic graphitization," Electrochimica Acta, vol. 173, pp. 50-58, 2015, doi: 10.1016/j.electacta.2015.05.042.
20. B.-K. Choi, W.-K. Choi, and M.-K. Seo, "Effect of catalytic graphitization on the electric heating performance of electroless nickel-coated carbon fibers," Current Applied Physics, vol. 42, pp. 86-91, 2022, doi: 10.1016/j.cap.2022.08.003.

21. E. H. Sujiono et al., "Fabrication and characterization of graphite powder based on coconut shell waste," Materials Today: Proceedings, 2021, doi: 10.1016/j.matpr.2020.11.749.
22. G. A. Zickler, B. Smarsly, N. Gierlinger, H. Peterlik, and O. Paris, "A reconsideration of the relationship between the crystallite size La of carbons determined by X-ray diffraction and Raman spectroscopy," Carbon, vol. 44, no. 15, pp. 3239-3246, 2006, doi: 10.1016/j.carbon.2006.06.029.
23. H. Qin et al., "Lignin-Derived Thin-Walled Graphitic Carbon-Encapsulated Iron Nanoparticles: Growth, Characterization, and Applications," ACS Sustainable Chemistry & Engineering, vol. 5, no. 2, pp. 1917-1923, 2017/02/06 2017, doi: 10.1021/acssuschemeng.6b02653.
24. K. N. b. T. Tanabe a, N. Tsukuda C and E. Kuramoto "On the characterization of graphite," Journal of Nuclear Materials, pp. 330-334, 1992.

PT. Mencerdaskan Bangsa Indonesia

PT MENCERDASKAN BANGSA INDONESIA (MBI), 4th Floor Gedung STC Senayan Room 31-34, Jl. Asia Afrika Pintu IX, Jakarta 10270, Indonesia.